2017

Microfluidic Enhanced Fabry-Perot Etalon Based Optical Biosensor for the Detection of Biological Substances in Liquid with Refractive Index Measurement

Nezam Uddin
South Dakota State University

MICROFLUIDIC ENHANCED FABRY-PEROT ETALON BASED OPTICAL BIOSENSOR FOR THE DETECTION OF BIOLOGICAL SUBSTANCES IN LIQUID WITH REFRACTIVE INDEX MEASUREMENT

BY

NEZAM UDDIN

A thesis submitted in partial fulfillment of the requirements for the

Master of Science

Major in Electrical Engineering

South Dakota State University

2017

MICROFLUIDIC ENHANCED FABRY-PEROT ETALON BASED OPTICAL BIOSENSOR FOR THE DETECTION OF BIOLOGICAL SUBSTANCES IN LIQUID WITH REFRACTIVE INDEX MEASUREMENT

NEZAM UDDIN

This thesis is approved as a creditable and independent investigation by a candidate for the Master of Science degree and is acceptable for meeting the thesis requirements for this degree. Acceptance of this thesis does not imply that the conclusions reached by the candidate are necessarily the conclusions of the major department.

Hyeun Joong Yoon, Ph.D. Date
Thesis Advisor

Steven Hietpas, Ph.D. Date
Head, Department of Electrical
Engineering and Computer Science

Dean, Graduate School Date

ACKNOWLEDGEMENTS

This thesis work was supported by Department of Electrical Engineering and Computer Science, South Dakota State University.

I have been supervised by Dr. Hyeun Joong Yoon throughout the graduate period. I would like to thank Dr. Hyeun Joong Yoon for his tremendous support in research work. I would like to mention Dr. Qi Hua Fan's contribution in initial period of my graduate study period and research work. I am also grateful to our group member's, Dr. Maheshwar Shrestha for his guidance and directions during the beginning of my research work. I would like to thank Kyugn Eun You, Shailu Poudyal, Mustafa Barnawi, and other students in the EE department, for their cordial support during this journey.

I don't want to forget to mention my family member's contribution to reach at this stage without whose love and support nothing would be possible.

TABLE OF CONTENTS

LIST OF FIGURES

LIST OF TABLES

ABSTRACT

MICROFLUIDIC ENHANCED FABRY-PEROT ETALON BASED OPTICAL BIOSENSOR FOR THE DETECTION OF BIOLOGICAL SUBSTANCES IN LIQUID WITH REFRACTIVE INDEX MEASUREMENT

NEZAM UDDIN

2017

A new microfluidic optical biosensor was demonstrated for refractive index measurements with high sensitivity and accuracy in the range of few micrometers liquid channels utilizing a Fabry-Perot cavity formed between two reflective semitransparent surfaces. The transmitted light through the cavity forms interference peaks in the transmission spectrum which is dependent upon the refractive index of the fluid in the microfluidic channel. We demonstrate the biosensor using Fabry-Perot to provide high accuracy and sensitivity with real-time measurement. The sensor can resolve refractive index changes with the shift of peak wavelength of transmitted spectrum. In our Fabry-Perot etalon based biosensor, two thin film coated glass substrates were used to detect the biological substances in liquid. Silver thin film is used on the glass substrates as the semitransparent layer to reflect the light repeatedly and cause interference of light. The SiO_2 layer coated on the silver layer created a hydrophilic surface in addition to protecting the silver layer from oxidation. The hydrophilic behavior of the SiO_2 films together with a capillary action allowed the tested liquids to easily flow into and wet the cavity between the two pieces of glass substrates. The device was utilized for measurement of the refractive index of sugar, glucose, potassium and sodium solution of different concentration at room temperature. The contact angle measurer, spectrophotometer and Dektak surface profilometer were used for characterization of the sensor. The proposed sensor has high

refractive index sensitivity, fast response, accurate, good linear response, and easy fabrication with super-hydrophilic microfluidic active layer. The result obtained from the experiment are in good agreement with the theoretical result and other reported result.

CHAPTER 1. INTRODUCTION

1.1. Background

The demand for detection of biological and chemical substances in liquid using the refractive index measurement is gradually increasing in different fields especially in medical and biology research applications [1, 2]. The nature of the liquid can be inferred by the refractive index property. Further, there is a relationship between the state of human biological systems and the refractive index of constituent fluids, such as glucose level in blood plasma is important for the management of diabetes [3]. Detection technique using the refractive index measurement is advantageous over many other detection techniques as it changes with the sample concentration/molecular interactions rather than sample volume/sample mass. Refractive index tells the total number of analytes present in the detection volume or on the detection surface irrespective of the amount of liquid. So the refractive index measurement based technique is useful even when ultrasmall (femtoliter to nanoliter) volume is involved [4]. Many other important parameters can be extracted from the refractive index which can be applied in the field of biology, chemistry, environment as well [5-7].

Accurate measurement of glucose level in blood is essential for the diabetic patients. The current glucose meters still need improvement in accuracy. Previous research confirmed that the glucose level could be determined by the refractive index of blood samples [8]. Therefore, optical spectroscopy is potentially accurate to measure glucose concentration because a small change in the refractive index can be directly detected from

optical interference. Detection of liquid concentration by using optical properties has gained popularity in medical fields.

There are two main steps for measuring the refractive index of liquid or gas: (1) detection of biomolecule/liquid and (2) the transduction into favorable signal. The detected signal can be transformed into convenient form by electrical, mechanical or optical means. Among the three transducing mechanisms of the label-free biosensors, the electrical conductance changes due to the binding of the receptors with the expected element and this change in conductance is realized by using CNTs or NWs. But the electrical liquid level sensors are confined their application in conductive or explosive liquid [9]. In mechanical transduction, the change in the surface stress in the cantilever surface is caused by the interaction between the two elements[10]. The most widely used transduction technique is the optical means such as surface plasmon resonance (SPR) [11-16], Raman spectroscopy [17], surface enhanced Raman spectroscopy (SERS) [18], localized SPR (L-SPR) [19-22], grating based refractive index sensors [6, 23, 24], liquid core ring resonator technology [25-27], photonic crystal nanostructured sensor [28-30], interferometer based sensor [10, 31, 32], optical waveguide based sensors [33, 34]**,** optical fiber based sensors [4, 35] etc. Refractive index measurement using these optical techniques have gained popularity over electrical and mechanical techniques due to some advantages such as small size, less weight, the sensor is not corrosive and gives accurate ignoring the effect of electromagnetic interference and mechanical disturbances, remote sensing capability, and multiplexed detection within a single device [4, 7, 36].

Most of the optical sensors are made of optical fiber whereas SPR, polymer based FPI sensors are mentionable other than optical fiber based liquid sensors. SPR has high accuracy, real-time responses, but it is costly, sensitive to the temperature and difficult to implement with the thin silver or gold film. Optical means of refractive index measurement using SPR, Total internal reflection (TIR) and leaky mode has potential in biological field. But the evanescent field intensity decreased with the thickness of the sensing medium when the light wave propagates at an interface. Optical interaction reduced at the sensor surface as merely few percent of the energy propagate in the sensing medium [37]. Metal layer is used in the sensing surface of SPR. The sensitivity of SPR sensors is not high due to the wide resonance dip in the reflectivity spectrum as light passes through lossy metal layer (higher k value) [38]. Porous layer, nanoparticle assembly can be used to increase the light matter interaction[39]. Leaky mode is needed to measure the higher refractive index and to include the entire particle interaction within the evanescent field of the sensor. A polymer nanostructured Fabry–Perot interferometer with microfluidic network has also been developed [10]. Although it increased the optical interaction with active layer up to 1-5 μm depth which is not possible by SPR, but the device structure is complex with nanopores, gold layer and PDMS layer. Photonic crystal sensors for detecting substances suffer from expensive nanofabrication processes, complicated and expensive optical setup for operation. Among the Optical fiber based refractive index sensors for detecting substances, such as fiber tapering [40, 41], fiber Bragg gratings (FBGs) [42, 43], long period gratings (LPFGs) [24], and core mismatch-based fiber sensing [40, 41], a single mode-multimode-single mode fiber structure[44], micro-bent fiber [45], multi-D-shaped fiber [46], open-cavity Fabry-Perot (FP) interferometers [47] are mentionable. Optical fiber

based refractive index sensors have some limitations. Nonlinear response, variation of result with temperature change, low range for higher sensitivity (grating based fiber), less mechanical strength and durability (tapered fiber sensors and core mismatch sensors), complex, precise and expensive fabrication procedure with phase masking and photolithographic procedures (FBG-based sensor), limited measurement accuracy, difficulty of miniaturization for multiple detection (LPFG-based sensors). Most of the optical fiber based sensors are sensitive to temperature change of surroundings. As the liquid filling process takes usually 6~16 minutes, the fiber based RI measurement of liquid is time consuming process. This time consumption can be reduced using pressure pump which is again a complex process [48]. Some fiber optic sensors are not a commercial product for the complex and costly fabrication process [40]. The cavity needs to be shortened for better performance. But it needs complicated techniques and increases fabrication cost.

As a refractive-index sensitive optical sensor, the transducing signal of a Fabry-Perot Etalon varies with the changes of the effective refractive index in its cavity. This property makes a Fabry-Perot Etalon an ideal technical platform for label-free bio sensing. Fabry-Perot etalon increases the sensitivity in terms of phase shift or absoption by creating unlimited effective interaction of light with material [49].

Although the Fabry-Perot fiber optic sensor overcome some limitations of other optical fiber based sensors mentioned above as it has complete overlap between the optical field and the medium being measured, still Fabry-Perot fiber optic sensor shows less satisfactory optical performance [5, 7]. Fabry-Perot interferometer based refractive index sensor

without optical fiber can overcome the problem of low RI sensitivity, nonlinear RI response, large temperature cross sensitivity [50], low field intensities as in fiber based sensor most of the light energy is contained in the fiber glass material resulting in evanescent-field based sensors . When Fabry-Perot technique is applied in fiber based sensor, it becomes bulky because of substrate/chip or microfluidic chip[3, 51]. Again sensor becomes more temperature sensitive because of the use of using multiple material [52]. We demonstrated a simple refractive index measuring technique based on Fabry-Perot etalon structure with microfluidic chamber made by two Ag/SiO_2 deposited glass substrates which can provide accurate, fast response with satisfactory sensitivity and resolution.

1.2. Previous Work

Various methods have already been developed to determine the refractive index of sugar, glucose, sodium and potassium in water. Practical range of glucose (200mg/dL to 700mg/dL) detection by a double-chamber Fabry-Pérot etalon [53]; high concentration of sodium chloride, glucose measurement using hollow glass prism [54], polarization sensitive optical low-coherence reflectometry to determine change in refractive index with different concentration of glucose, KCl, NaCl [55]; glucose detection using U-Shaped Bending-Induced Interference Optical Fiber Sensor [56]; phase-sensitive optical low-coherence reflectometry (PS-OLCR) to measure the change of refractive index with glucose, sodium chloride, potassium chloride [57]; differential phase optical coherence tomography (DP-OCT) to measure the refractive index of different concentration of glucose, sodium chloride, potassium chloride [58], a refractometer based on a long-period-

grating fiber to measure the refractive index of sugar solutions [59]; surface plasmon resonance [54, 60] or fiber optics based sensors [61-64] were also reported, showing promising results in detecting the sugar levels in water solutions. In those reported methods, either the device fabrication was complicated or the signal intensity needed to be improved. Some methods require two step measurements with reference measurement [46], suffer from less accuracy [47], needs complex experimental set up [48]; provides low signal [49], needs costly optical experimental set up [50] [51]. So, there is a need of sensors for fast response, mechanically strong, highly sensitive, can provide real time response with easy fabrication and optical set up.

The problems of different types of sensors discussed earlier can be overcome by the proposed Fabry-Perot Etalon made of two reflective glass substrates. Fabry-Perot etalon has been demonstrated to be potentially simple and accurate for measuring the refractive indices of liquids[7, 36, 65]. Most of the Fabry-Perot-type sensors for detecting chemical or biological substances in liquid were based on optical fibers[66], in which the interference occurred due to light reflection between two surfaces of a thin-cut slot in a fiber. As the reflectance at the fiber/air interface was relatively low (a few percent only), the sensitivity of these devices was not satisfactory.

The applications of Fabry-Perot have made our sensor an accurate approach to measure the refractive index of liquid. The microfluidic structure will eliminate the need of auxiliary pressure equipment to facilitate the liquids getting into and out of the sensor [50]. The integration of microfluid channel and light matter interaction has the potential in detecting the biological substance accurately with small volume of sample [3]. This work

demonstrated that thin silver (Ag) coatings could greatly enhance the interference and the sensitivity of Fabry-Perot etalons for detecting the refractive index of liquids. The greatly enhanced performance is based on the unique optical properties of Ag thin films: 1) low absorption loss in visible spectrum range, and 2) adjustable reflectance/transmittance by varying the film thickness over 10-20 nm. However, a thin Ag films is sensitive to the environment (e.g. oxygen). Ag thin-film surface oxidizes if it is exposed to air[67, 68]. Another drawback of Ag surface is the low wettability; a metal surface is usually not hydrophilic, which restricts the flow of liquid and hinders the use of Ag-based etalon for measuring liquids [69]. On the other hand, a hydrophilic surface could be achieved by using a dielectric or metal oxide layer [70]. The dielectric layer can also protect the Ag film from being oxidized.

In this report, we introduce a simple Fabry-Perot etalon based sensor with high accuracy integrated into a micro- fluidic geometry containing the fluid to be tested. The variation of refractive index of the fluid in the microfluidic channel changes the peak wavelength in the transmittance spectrum. We demonstrate this refractometer using two layers of Ag thin films to form the reflective surface and create interference. In our sensor structure, Ag layer is used to reflect the light source and produce interference. We considered the response of a Fabry-Perot sensing interferometer with thin semi-transparent Ag layers deposited on the two glass substrates and using Al spacer to form the cavity, transmittance interference signal was acquired by thin film analyzer while the length of the air cavity was fixed. By measuring the changes of analyte refractive index (RI), the label-free biological detection can be realized with high sensitivity and fast response. In this

paper, the refractive index of sugar, glucose, NaCl and KCl solution has been measured from the change of peak wavelength of the transmittance spectrum with respect to air from the sensor.

1.3. Motivation

Need for fast response, mechanical strength, high sensitivity, real-time response, easy fabrication and less complex optical set up for biological substances detection using optical properties.

1.4. Objectives

To Fabricate Fabry-Perot Etalon optical sensor by easy and low-cost process, to investigate the theoretical validation of this type of sensor and simulate the result using appropriate method. In addition, to fabricate the sensors and apply it in the measurement of liquid response. For completing the above-mentioned objectives, the following steps were performed.

- *Fabry-Perot Etalon Biosensors*
    - Model micro cavity Fabry-Perot using the Macleod Software
    - Design and fabricate Ag thin film based Fabry-Perot sensors
    - Test Fabry-Perot sensors for liquid with different sugar, glucose, NaCl, KCl levels.

- Modified Fabry-Perot Etalon
    - Modify micro cavity sensors with SiO_2 protective layers
    - Develop theoretical model for modified micro-cavity Fabry-Perot
    - Improve hydrophilic surface
    - Identification, deposition and testing of active layers

- Fabry-Perot etalon Glucose sensor with microfluid channel

- Fabricate microfluidic based Fabry-Perot etalon optical sensor to improve the performance.

CHAPTER 2. THEORY

2.1. Properties of Light

2.1.1. Electromagnetic Light Wave

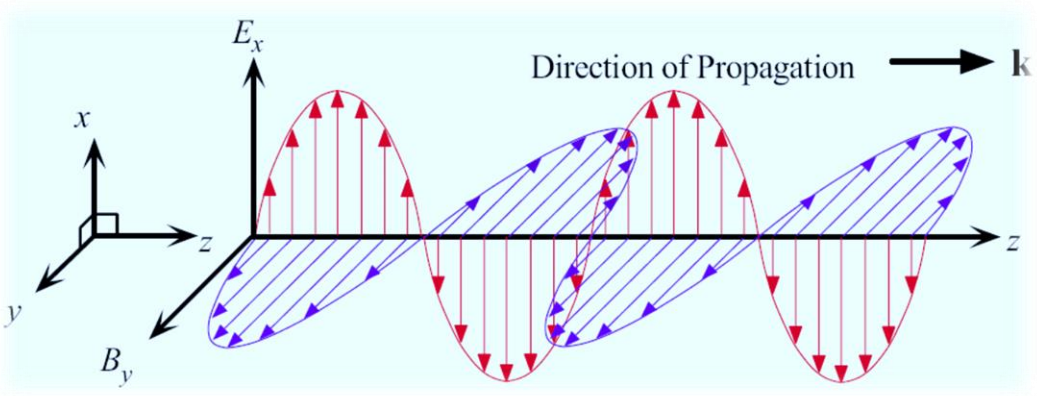

Figure 2. 1 Propagation of Electromagnetic wave [71]

Light is an Electromagnetic wave. Electromagnetic wave which is a traveling wave has two components. The time-varying electric and magnetic fields that are perpendicular to each other along x and y direction while the wave propagates along z direction.

Electromagnetic wave propagating in the z direction has an electric field propagating in the x direction and magnetic field in the y direction propagating as shown in figure 2.1. Wave Amplitude is a function of position (z) and time (t). The electric field can be expressed as

$$E_x = E_0 \cos(\omega t - kz + \phi_0) \qquad 2.1$$

E_x= electric field along x at position z at time t

$k = 2\pi n/\lambda$, propagation constant

λ = wavelength

ω = angular frequency

E_0 = amplitude of the wave

ϕ_0 is a phase constant which accounts for the fact that at $t = 0$ and $z = 0$, E_x may or may not necessarily be zero depending on the choice of origin.

$(\omega t - kz + \phi_0) = \phi$ = phase of the wave

This equation describes a monochromatic plane wave of infinite extent traveling in the positive z direction

2.1.2. **Phase Velocity**

The time and space evolution of a given phase ϕ, for example that corresponding to a maximum field is described by

$\phi = \omega t - kz + \phi_0$ = constant

During a time interval δt, this constant phase (and hence the maximum field) moves a distance δz. The phase velocity of this wave is therefore $\delta z/\delta t$.

The **phase velocity *v* in vacuum** is

$$v = \frac{dz}{dt} = \frac{\omega}{k} = f\lambda \qquad 2.2$$

where f is the frequency ($\omega = 2\pi f$).

2.1.3. **Light at Materials Interface**

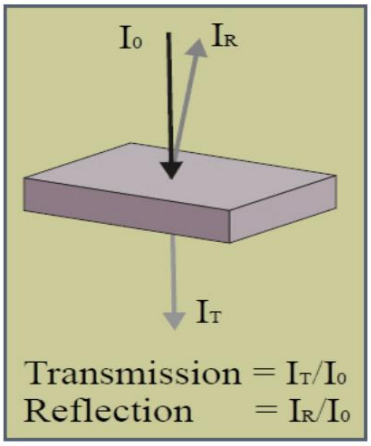

Figure 2. 2 propagation of light through material [72]

When light is incident at a material surface, part of the light will be reflected and rest transmits considering no absorption. Reflection is caused at an interface by differences in refractive index between two mediums as for example Air to glass, Glass to Silicon, etc. The multiple reflected rays overlap with each other and occur interference.

2.1.4. **Propagation of Light at an Interface**

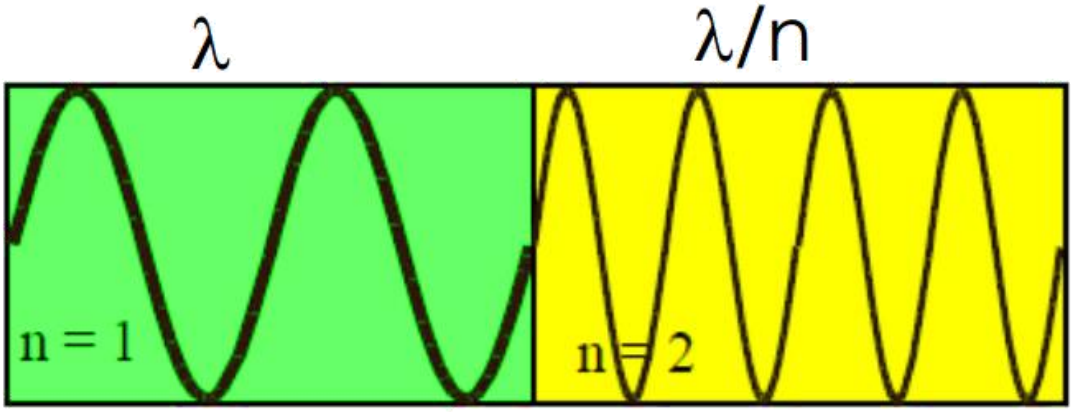

Figure 2. 3 Propagation of light waves in two different mediums [72]

When light transmits from one medium to other medium, the velocity and wavelength vary in dissimilar materials. The velocity of light waves in any medium is

$$v = \frac{c}{n} \qquad 2.3$$

The wavelength λ of light waves in air turns into $\frac{\lambda}{n}$ when light passes throght any medium having refractive index of n other than air/vacuum. But the frequency of wave remains the same.

$$\vartheta = \frac{v}{\lambda} \qquad 2.4$$

2.1.5. **Refractive Index**

When an electromagnetic field is travelling in a dielectric medium, the oscillating electric field polarizes the molecules of the dielectric material at the frequency of the wave. The polarization mechanism delays the propagation of the electromagnetic waves. Electromagnetic wave velocity reduces due to this reason. The stronger the interaction of light and material, the slower the propagation of wave. The relative permittivity ϵ_r measures the extent of interaction between light and induced dipoles. Light propagates slowly in a denser medium having higher refractive index value. Refractive index is the ratio of the velocity of light *c* at a given wavelength in empty space with respect to its velocity *v* in a substance, or $n = c/v = \sqrt{\epsilon_r}$. If the number of molecules per unit volume increases which in turn increases the polarizability. If the polarizability increases the refractive index also increases. In another word, it is equal to the impediment to propagation of light where

Speed in vacuum: c = $\frac{1}{\sqrt{\mu_0 \epsilon_0}}$ =3x10^8 m/s

Wave speed in material = c/n

Some typical refractive indices of different mediums are vacuum = 1, air=1.0003, water = 1.33, glass= 1.50

2.1.6. **Light Reflection & Refraction**

When light is incident on a surface at an angle, part of the light will be reflected and rest transmits. Reflection happens due to having different refractive index values of two mediums at an interface. The transmitted light changes path when it moves from one medium to another.

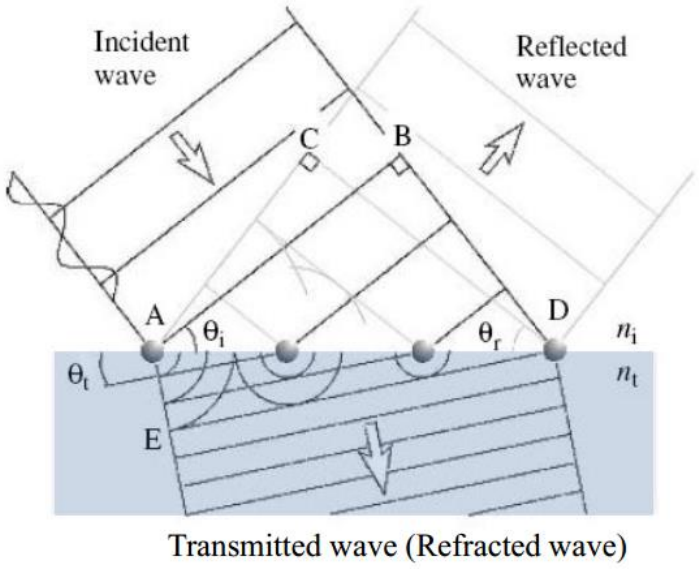

Figure 2. 4 Light reflection and refraction [72]

The angle of refraction can be found from the Snell's Law

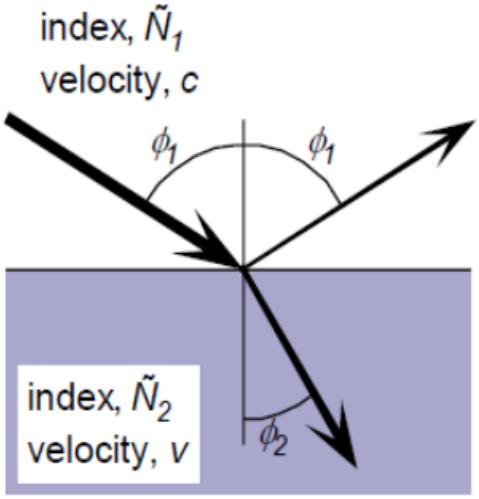

Figure 2. 5 Light bending between two different mediums [72]

For reflection(Specular) phenomena, incident and reflection angles are equal.

$$\varphi_i = \varphi_r \quad (2.5)$$

For the refraction (Snell's Law), the bending of light occurs.

- for dielectrics, i.e., k = 0

$$n_1 sin\varphi_1 = n_2 sin\varphi_2 \quad (2.6)$$

- in general, (Adding Absorption)

$$N_1 sin\varphi_1 = N_2 sin\varphi_2 \quad (2.7)$$

Where N_1 and N_2 are complex refractive index.

2.1.7. **Fresnel's Equations**

The incident, reflected & refracted waves can be expressed with the exponential form of a traveling plane wave, i.e.

Incident wave: $E_i = E_{i0} \exp j(\omega t - K_{ir})$

Reflected wave: $E_r = E_{r0} \exp j(\omega t - K_{rr})$

Transmitted wave: $E_t = E_{t0} \exp j(\omega t - K_{tr})$

As a requirement of electromagnetic wave theory, electric and magnetic fields anywhere on the wave must be perpendicular to each other. $E_{\parallel}$ (p-wave) in the EM wave associates a magnetic field $B_{\perp}$ such that, $B_{\perp}$=(n/c) $E_{\parallel}$. Similarly, $E_{\perp}$ (s-wave) will associate magnetic field $B_{\parallel}$ such that $B_{\parallel}$=(n/c) $E_{\perp}$.

We use boundary conditions

$$E_{tangential(1)} = E_{tangential(2)} \quad (2.8)$$

$$B_{tangential(1)} = B_{tangential(2)} \quad (2.9)$$

The amplitudes of the reflected and transmitted waves can be obtained in terms of n_1, n_2 and the incident angle θ_i by applying the boundary conditions to the EM wave going from medium 1 to 2 using the Maxwell equation. These relationships are called Fresnel's equations.

Define $n = n_2/n_1$

Reflection and transmission coefficients for $E_{\perp}$ are

$$r_{\perp} = \frac{E_{ro,\perp}}{E_{io,\perp}} = \frac{\cos\theta_i - [n^2 - sin^2\theta_i]^{1/2}}{cos\,\theta_i + [n^2 - sin^2\theta_i]^{1/2}} \quad (2.10)$$

$$t_{\perp} = \frac{E_{to,\perp}}{E_{io,\perp}} = \frac{2\cos\theta_i}{cos\,\theta_i + [n^2 - sin^2\theta_i]^{1/2}} \quad (2.11)$$

There are corresponding coefficients for the $E_{||}$ fields with corresponding reflection and transmission coefficients, $r_{||}$ and $t_{||}$

$$r_{||} = \frac{E_{ro,||}}{E_{io,||}} = \frac{[n^2 - sin^2\theta_i]^{1/2} - n^2 \cos\theta_i}{[n^2 - sin^2\theta_i]^{1/2} + n^2 \cos\theta_i} \quad 2.12$$

$$t_{||} = \frac{E_{to,||}}{E_{io,||}} = \frac{2n \cos\theta_i}{[n^2 - sin^2\theta_i]^{1/2} + n^2 \cos\theta_i} \quad 2.13$$

For normal incidence (θ_i = 0), Fresnel's equations are

$$r_{||} = r_{\perp} = \frac{n_1 - n_2}{n_1 + n_2} \quad 2.14$$

2.1.8. **Intensity, Reflectance and Transmittance**

Reflectance R measures the intensity of the reflected light with respect to that of the incident light. It can be defined separately for electric field components parallel and perpendicular to the plane of incidence.

The reflectance $R_{||}$ and $R_{\perp}$ are defined by

$$R_{\perp} = |r_{\perp}|^2 \quad 2.15$$

$$R_{||} = |r_{||}|^2 \quad 2.16$$

For normal incidence

$$R = R_{||} = R_{\perp} = \left(\frac{n_1 - n_2}{n_1 + n_2}\right)^2 \quad 2.17$$

Transmittance T relates the intensity of the transmitted wave to that of the incident wave in a similar fashion to the reflectance. We must, however, consider that the transmitted wave is in a different medium and further its direction with respect to the

boundary is also different by refraction. For normal incidence, the incident and transmitted beams are normal and the transmittances are defined and given by

$$T_{\perp} = \frac{n_2}{n_1}|t_{\perp}|^2 \qquad 2.18$$

$$T_{||} = \frac{n_2}{n_1}|t_{||}|^2 \qquad 2.19$$

For normal incidence

$$T = T_{||} = T_{\perp} = \frac{4n_1n_2}{(n_1+n_2)^2} \qquad 2.20$$

Further, the fraction of light reflected and fraction transmitted must add to unity. Thus, *R* + *T* = 1 for non-absorption medium

2.1.9. **Absorption and Extinction**

When light propagates from one medium to another lossy/absorbing medium, wavelength changes to λ/n and speed changes to c/n while the frequency does not change and the amplitude decreases with depth

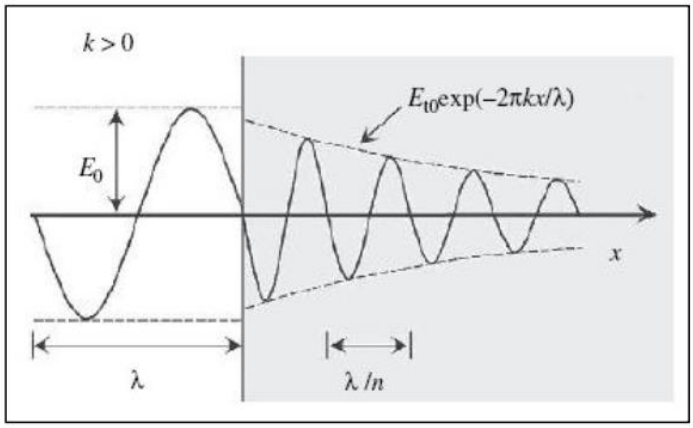

Figure 2. 6 **Light propagation through an absorbing medium [72]**

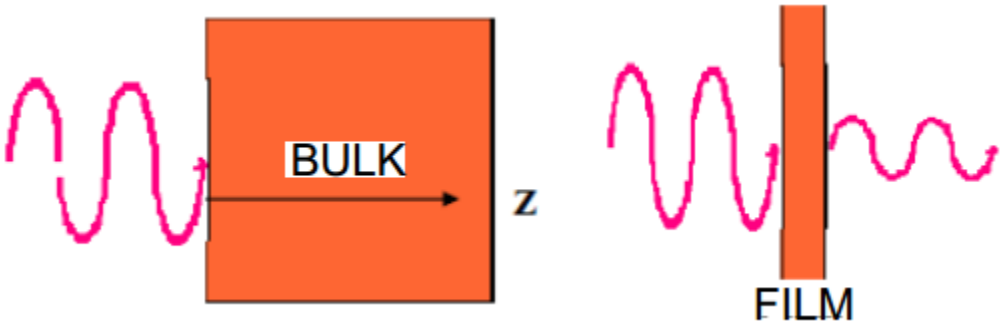

Figure 2. 7 **Absorption of light through a bulk material and thin film [72]**

The intensity of light at a depth with absorption

$I = I_0 e^{-i\propto z}$ where $\propto = \frac{4\pi k}{\lambda}$

When light is absorbed by Bulk Materials that means light should propagate at a deeper distance which gives more energy loss and complete extinction.

For the absorbing films, increasing thickness gives longer propagation path in film, wave spends longer time in film, more absorption by material as well as more extinction of wave.

2.1.10. **Optical Refraction & Absorption**

When Light travels through a medium with refractive index greater than 1, it "slows down". Refraction changes direction of propagation and absorption can also occur when $k > 0$.

The main causes of absorption in metals, semiconductors are Free Electron Absorption, Resonant Absorption, Bound electrons driven by wave and for Oscillating electron clouds; Heat Losses are the reason for absorption in dielectric.

2.1.10.1. Metals: Refractive Index

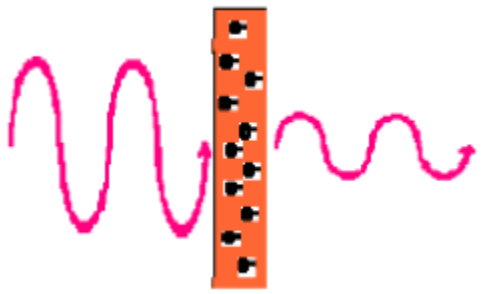

Figure 2. 8 **Absorption phenomena in metals [72]**

As metals have large number of free electrons and the "Extra" electrons not shared are set "free" by the atoms. Those electrons travel freely in the material and absorb Light. Free electrons also give Electrical conduction, and Optical absorption. The

applied field of light wave causes electrons to move and the applied wave energy is lost as heat.

2.1.10.2. Dielectrics: Refractive Index

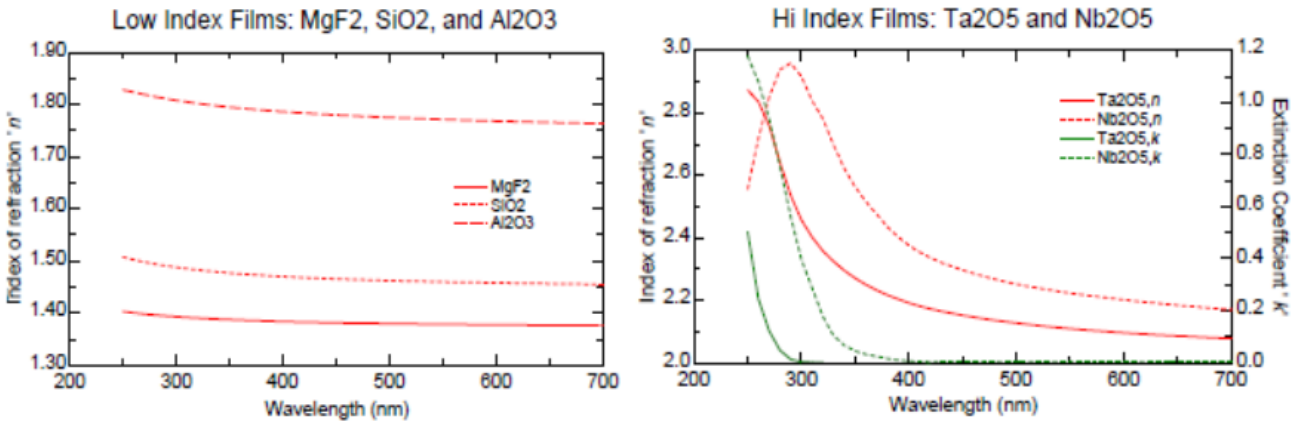

Figure 2. 9 **Absorption in dielectric material [72]**

Dielectric materials are transparent at visible & near infrared wavelengths. Absorption occurs in UV (Sometimes deep UV) and Low index materials are transparent into UV or VUV. Materials with High index absorb light at longer wavelengths.

The change of refractive index with wavelength λ is known as DISPERSION.

2.1.11. **Thin Film Interference**

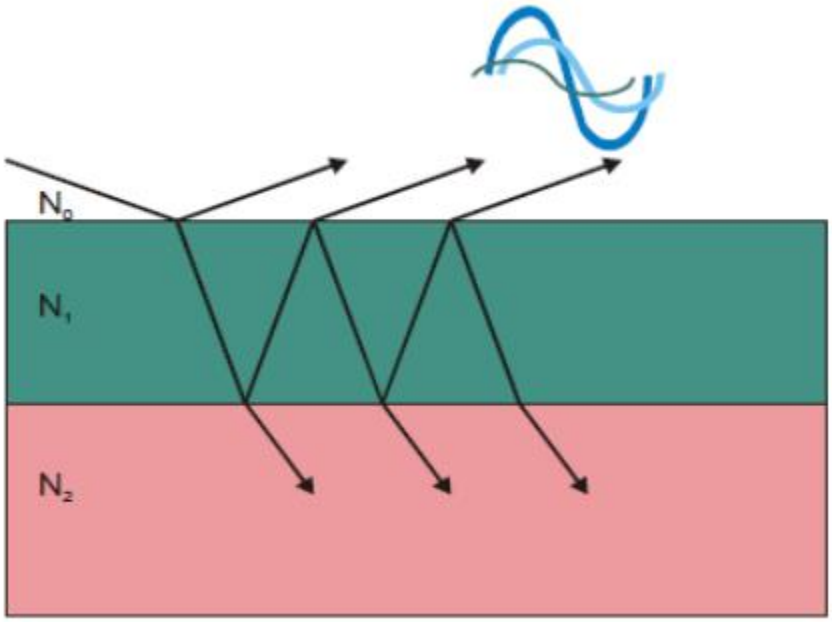

Figure 2. 10 **Interference of light in thin film [72]**

Interference between the waves reflected from the top and bottom of a film is the thin film interference. Each reflected wave will have a different phase and amplitude. All multiple reflections add up to establish a single reflected polarization state which can be measured at detector.

2.1.12. **Fabry-Perot Etalon:**

The Fabry-Perot interferometer is an optical instrument which uses multiple-beam interference. The basic structure of Fabry-Perot Etalon is two reflecting mirror in which each beam of light interferes with each other and causes interference.

2.2. Principle of Fabry-Perot Etalon

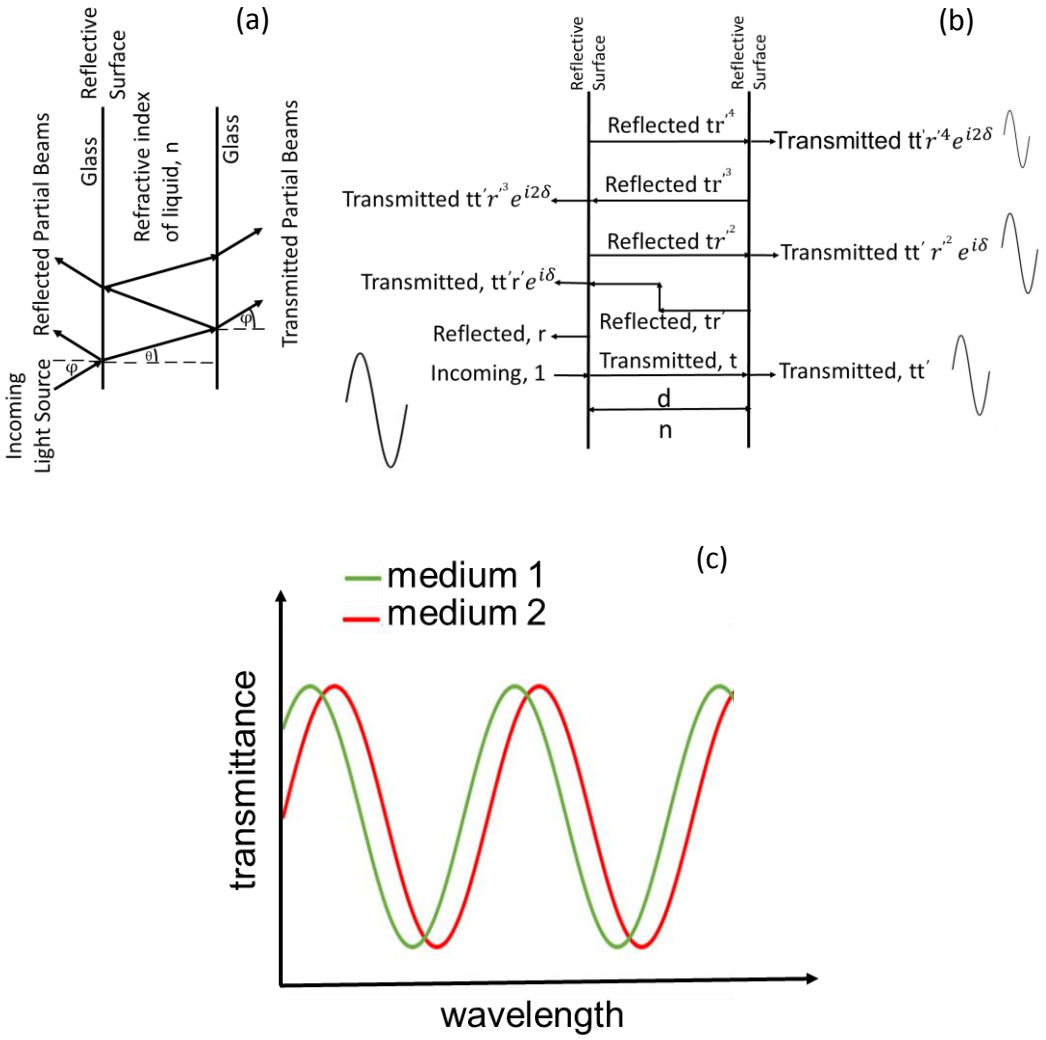

Figure 2. 11 **(a) Simple Fabry-Perot etalon structure (b) Calculation of the reflected and transmitted wave (c)Transmittance spectra from the sensor for two different mediums**

A basic Fabry-Perot etalon consists of two closely spaced partially reflective surfaces as shown in FIG. 2.12 (a,b) [73]. When light travels to the reflecting surfaces, part of the light is reflected and part is transmitted. Multiple offset beams interfere with each other. The interference is periodic in wavelength (Fig. 2.12(c)). Although the transmission

and reflection in the proposed modified Fabry-Perot etalon is more complicated, the basic theory discussed here is applicable.

The transmitted electric field from the two semitransparent reflective surfaces differ from each other by magnitude and phase angle which depends on the thickness of the Ag layer on glass substrates. The transmitted and reflected light intensities I_t and I_r can be found from the summation of the amplitudes of the respective waves. The transmission and reflection co efficient from glass to medium n is indicated by t and r while for opposite travel of light these co efficient are r' and t' as shown in Fig. 2.13.

Relations between the reflectance and transmittance values for amplitudes can be derived using time reversal invariance. The incoming light energy and outgoing light energy will be conserved at an interface neglecting the absorption. Fig. 2.14 shows the 'normal' and the reversed light ray propagation through a surface and denotes the corresponding amplitudes.

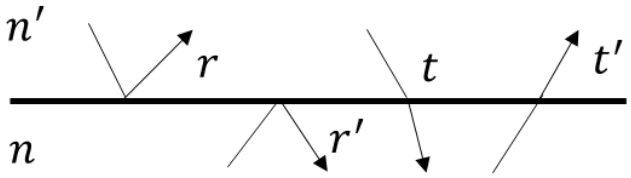

Figure 2. 12 Transmission and reflection co efficient illustration between two mediums

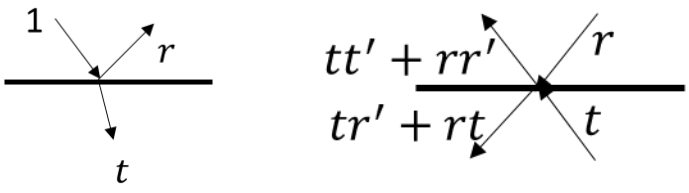

Figure 2. 13 Transmission and reflection co efficient for Normal and time reversed at the interface

After the application of the concept of transmission and reflection co-efficient at the interfaces of two different mediums

$$tt' + rr = 1 \qquad 2.\ 21$$

$$tr' + rt = 0 \qquad 2.\ 22$$

Therefore

$$R' = -r,\ r'^2 = r^2 = R^2 \quad tt' = T = 1 - R \qquad 2.\ 23$$

The phase of each transmitted wave differs from that of the preceding wave by an amount corresponding to the difference in their paths. For example, the optical paths of 2nd and 1st waves (Fig 2.12 (b)) of Fabry-Perot etalon differ by 2ndcosφ.

The phase difference δ corresponds to the path difference. The phase difference between two consecutive rays is given by

$$\delta = \frac{2\pi nd\cos\theta}{\lambda} \qquad 2.\ 24$$

where d is the distance between the two semitransparent glass substrates, θ is the transmission angle, n is the refractive index of the medium and λ is the wavelength of light source.

The incident electric field of a plane wave is of the form

$$E(t) = E_0 e^{-i\omega t + ikz} \qquad 2.\ 25$$

where k = 2πn/λ and z is the distance of propagation. For the incident wave, let us assume z = 0. For simplification, let us assume E_0 to be unity. Then

$$E_{inc} = e^{-i\omega t} \quad 2.\ 26$$

The 1st transmitted field will be

$$E_{t1} = tt'e^{-i\omega t} \quad 2.\ 27$$

The 2nd transmitted wave will be

$$E_{t2} = tt'r'r'e^{i\delta}e^{-i\omega t} \quad 2.\ 28$$

The rest of the infinite rays will be as follows

$$E_{t3} = tt'r'^4e^{i2\delta}e^{-i\omega t} \quad 2.\ 29$$

.
.
.
.

Each time there will be a reflected and transmitted ray and the sum of all infinite transmitted electric fields is

$$E_{trans} = (tt' + tt'r'r'e^{i\delta} + tt'r'^4e^{i2\delta} + tt'r'^6e^{i3\delta} + \cdots)e^{-i\omega t} \quad 2.\ 30$$

The ratio of transmitted to incident electric fields amplitude will be

$$\frac{E_{trans}}{E_{inc}} = tt' + tt'r'r'e^{i\delta} + tt'r'^4e^{i2\delta} + tt'r'^6e^{i3\delta} + \cdots \quad 2.\ 31$$

In a lossless system, and with *r = r'* for identical etalon surfaces, this equation simplifies to

$$\frac{E_{trans}}{E_{inc}} == \frac{tt'}{1-r^2e^{i\delta}} = \frac{1-r^2}{1-r^2e^{i\delta}} = \frac{1-\boldsymbol{R}}{1-\boldsymbol{R}e^{i\delta}} \quad 2.\ 32$$

where *r* and *t* are the reflection and transmission coefficients for the light travelling from the air to the medium having refractive index *n*, respectively. Similarly, for light travelling in the reverse direction, the reflection and transmission coefficients are r' and t', respectively. The reflectance R can be expressed in terms of the coefficient as $R= |r|^2=|\frac{n-1}{n+1}|^2$ where *n* and 1 are refractive indices of each medium, assuming the wave propagates from air to medium of refractive index of n.

The transmittance, *T*, is the ratio of the transmitted and incident light intensities which is the square of the field wave.

$$T = \frac{(1-\boldsymbol{R})^2}{1+\boldsymbol{R}^2-2\boldsymbol{R}cos\delta} = \frac{(1-\boldsymbol{R})^2}{1+\boldsymbol{R}^2-2\boldsymbol{R}+2\boldsymbol{R}(1-cos\delta)} = \frac{(1-\boldsymbol{R})^2}{(1-\boldsymbol{R})^2+4\boldsymbol{R}sin^2(\delta/2)} \quad 2.\ 33$$

This can be written in the form

$$T = \frac{1}{1+Fsin^2(\delta/2)} \quad 2.\ 34$$

Where F is the coefficient of finesse

$$F = \frac{4\boldsymbol{R}}{(1-R)^2} \quad 2.\ 35$$

This function is known as the Airy function

The frequency at which the transmission peak will occur;

$$\upsilon_m = \mathrm{m}\frac{\mathrm{c}}{2\mathrm{nlcos}\theta} \quad 2.\ 36$$

where m= any integer

The separation of the frequency between two successive transmission peaks are known as free spectral range (FSR).

$$\mathrm{FSR} = \Delta\upsilon = \upsilon_{m+1} - \upsilon_m = \frac{c}{2nl\cos\theta} \qquad 2.37$$

From the transmission spectrum of the Fabry-Perot etalon, the refractive index of the analyte in the cavity can be extracted using the above-mentioned equation.

In our proposed structure, a special condition has been applied where the light incident at the normal direction of the surface. For different medium in the cavity, the transmittance spectrum will be different with a clear shift of peak transmittance wavelength (Fig. 2.12). From the shift of wavelength, the refractive index of liquid can be found.

Each sensor can be first calibrated by measuring the transmission spectrum with an air gap, which has a known refractive index of 1. Using Equation 2.37, the gap thickness *d* can be deduced from the transmission peak positions. Once *d* is known, a liquid sample with unknown refractive index can be injected into the gap. Measuring the transmittance again will provide another spectrum that has different peak positions as compared with the air gap. Since *d* will not change, the new peak positions can be used to deduce the refractive index of the liquid.

2.3. Matrix Method for Multilayers Fabry-Perot Sensors

Our proposed sensor contains two reflective layers, two dielectric layer on glass substrate with the cavity. The calculation for only two reflective layers has been shown in 2.2 section but for a multiple film stacks, calculation of the overall reflectance and transmittance becomes very complicated. Because multiple reflections occur at every interface in the film stacks. Optical characteristics of the multiple films can be

investigated by the characteristic matrix method. In this method, each film is represented by a 2*2 matrix, called characteristic matrix. The characteristic matrix includes effects of the thickness of the deposited layer and the refractive index of each thin film. The optical characteristics of the multiple film stacks can be calculated using a product of all the characteristic matrix.

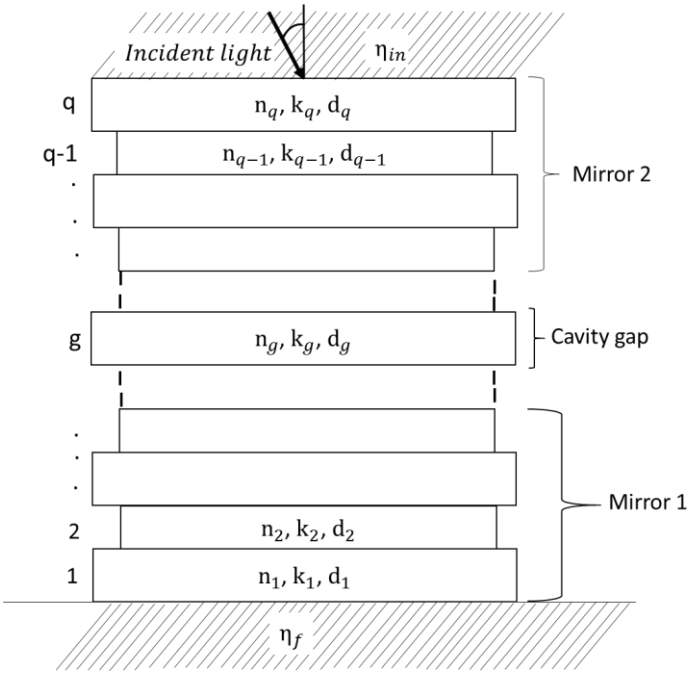

Figure 2. 14 Schematic diagram of multiple layer Fabry-Perot Etalon Sensor

Fabry-Perot etalon of multiple films is shown in Figure 2. 14 consisting of q layers. Two mirrors are consisted of multiple films and the g layer has been shown as the cavity gap. Each layer is characterized by the refractive index, film thickness and phase thickness. Each layer has refractive index of n_i which can be complex and consisting of n and k value, $\tilde{n}_i = n_i' - jk_i'$ to represent a lossy medium. The admittance of each layer can be found from the refractive index of each layer and the admittance in vacuum i.e, $\eta_i = Y_o.\tilde{n}_i$ where Y_o is the vacuum admittance (1/377 siemens). Suppose a plane wave with

wavelength (λ_0) in vacuum is propagating into the Fabry-Perot cavity at normal incidence.

The characteristic matrix at a wavelength λ for the assembly of N layers is given by

$$M = M_1 M_2 \ldots\ldots M_N \ldots\ldots \quad 2.\ 38$$

Each layer is represented by a characteristics matrix of 2×2 M, of the form

$$M_j = \begin{pmatrix} cos\delta_j & \frac{isin\delta_j}{\eta_j} \\ i\eta_j cos\delta_j & cos\delta_j \end{pmatrix} \quad 2.\ 39$$

where n_i is the refractive index of the i[th] layer and δ_i is its phase thickness given by $\delta_i = 2\pi n d_j/\lambda$ with the physical thickness of the layer being d_j.

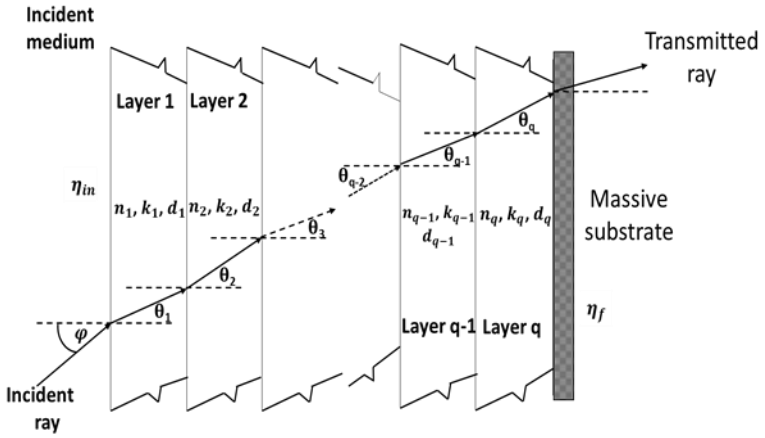

Figure 2. 15 Propagation of light in a multilayer Fabry-Perot Etalon

Using the equivalent characteristic matrix M the transmittance T of this structure is calculated using

$$T = \frac{|2\eta_{in}\eta_f|}{|\eta_{in}B+C|^2} \quad 2.\ 40$$

where,

$$\begin{bmatrix} B \\ C \end{bmatrix} = M. \begin{bmatrix} 1 \\ \eta_f \end{bmatrix} \quad 2.41$$

$\eta_{in}$and η_f are the admittances of the medium for incoming light and outside of the sensor (the substrate in this case), respectively.

2.4. Sputtering

Sputtering is the technology of removing material from the source and deposit thin films in the substrate. The mostly used techniques of sputtering are DC sputtering for metal and RF sputtering for metal, insulator and dielectric material. Sputtering is the alternative approach of evaporation. In DC sputtering the potential is applied directly to the target material from which the material is released to deposit on the substrate. But in case of dielectric material or insulator material, the potential cannot be applied directly in the target. This problem can be overcome by applying a high frequency potential to a metal electrode behind the insulator. Power is fed into the plasma through the dielectric material, and sputtering can occur because the insulator will now be alternately ion and electron bombarded. The source material (target) and substrate is placed inside the vacuum chamber and inert gas (argon) is introduced in the vacuum chamber at a low pressure. A gas plasma is struck using an RF power source which is a high voltage RF source, causing the gas to become ionized. A matching network is utilized to optimize power transfer from the RF source to the plasma. Ions are accelerated towards the surface of the target, causing atoms of the source material to break off from the target in vapor form and condense on all surfaces including the substrate as shown in figure 2.17. As for evaporation, the basic principle of sputtering is the same for all sputtering technologies.

The differences typically relate to the way the ion bombardment of the target is realized.

A schematic diagram of a typical RF sputtering system is shown in the figure 2.18.

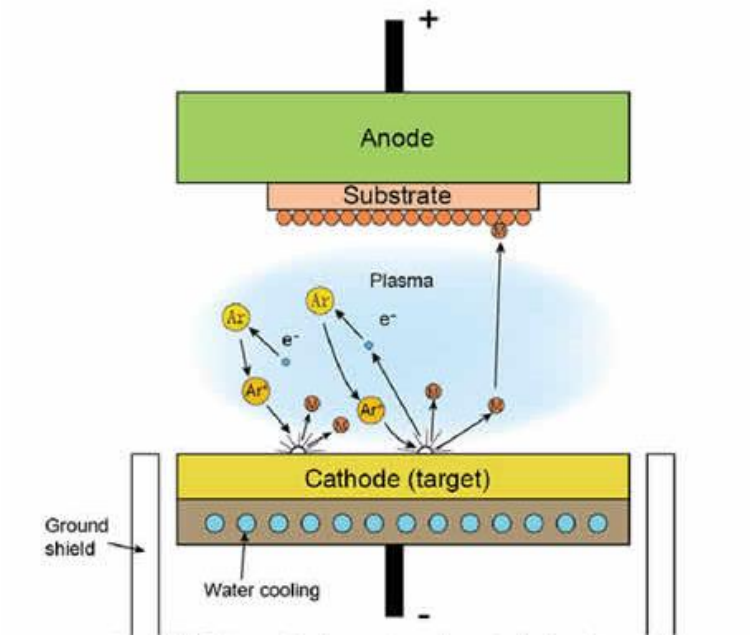

Figure 2. 16 Working principle of sputtering [74]

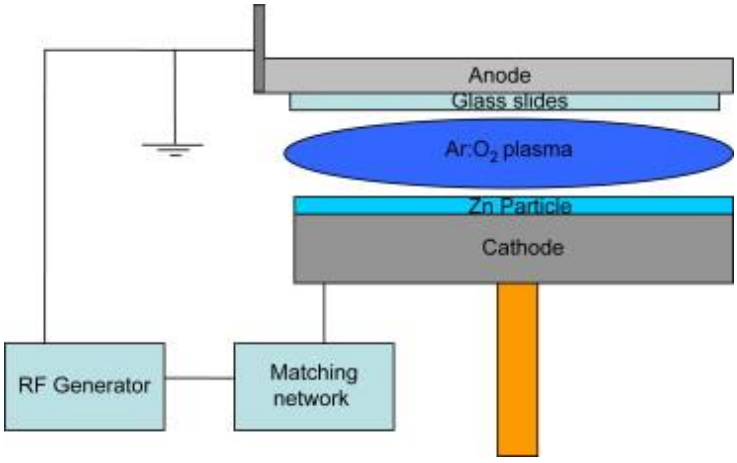

Figure 2. 17 Schematic drawing of the RF sputtering system [75]

2.5. Electro Discharge Machining

The process of removing material from the work piece by the mechanism of anodic dissolution during an electrolysis process is known as the Electro discharge machining (EDM) which is a nontraditional machining process. D.C. voltage of 10-25 volts is applied between the anode(workpiece) and cathode (pre-shaped tool) to be appeared across the inter-electrode gap. The electrolyte flows through the inter-electrode gap of between 0.1-0.6 mm. The current density is usually 20 to 200 Amperes per cm square. The rate of removing by EDM process depends on some factors such as the anodic dissolution rate, which is governed by Faraday's laws of electrolysis, electrochemical properties of the metal, electrolyte properties and electric current/voltage applied. EDM can generate an approximately the same pattern of the tool on the workpiece. EDM has been applied in many industrial applications including turbine blades, engine castings, bearing cages, gears, dies and molds and surgical implants[76-78].

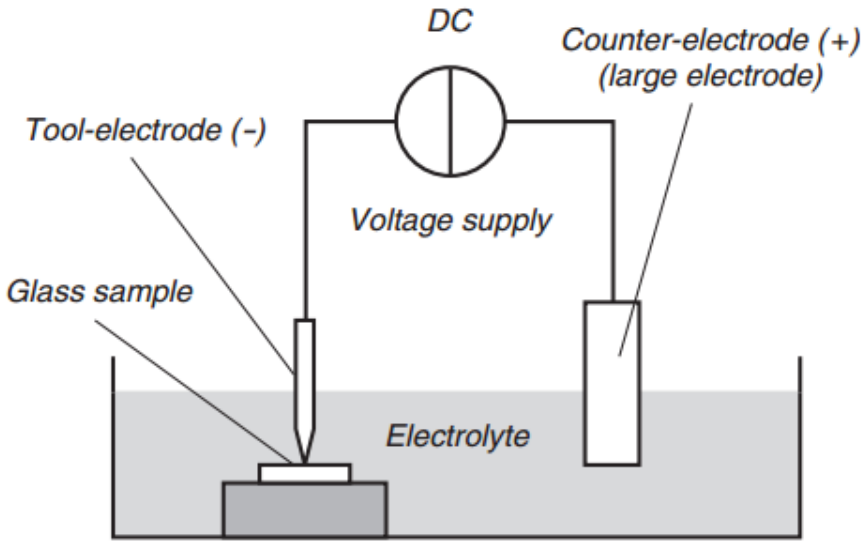

Figure 2. 18 Experimental set up of EDM [79]

2.6. Profilometer Dektak

The Dektak is a stylus (contact) profilometer is used to measure the thickness of the thin film. The thickness profile can be found when stylus makes physical contact with the surface of the thin film and move from one point to another to measure the difference of surface height. The scanner of dektak is placed in a dark plastic case on an isolated platform so that the measurement does not contain any ambient disturbances. A software is used to control the stage and to move the stage to get the surface profile.

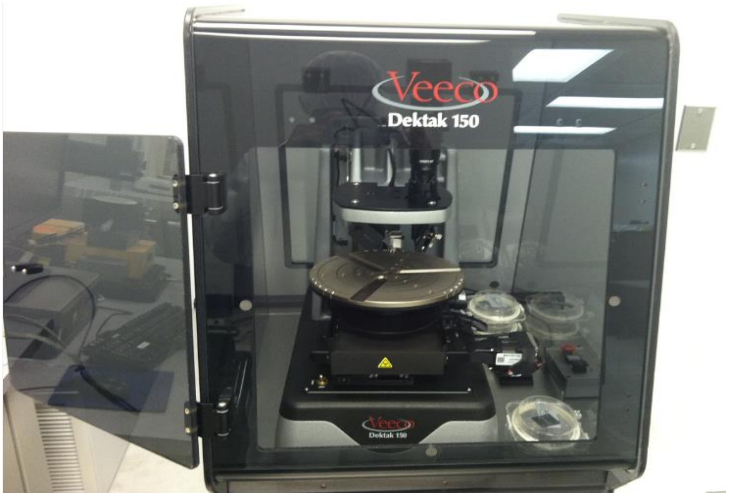

Figure 2. 19 Dektal Profilometer [80]

2.7. Buffered Oxide Etchant

BOE is the short name for "Buffered Oxide Etch", which is a mixture of ammonium fluoride, HF, and water. BOE is used to remove the oxide layer of silicon wafer, unwanted silicon di oxide portion in the lithography process or even to etch the glass substrate. Ammonium fluoride is highly soluble in water (concentrated ammonium fluoride is approximately 40% by weight in water). In the BOE etchants, the ammonium fluoride is basically a buffer which maintains the pH of the solution to keep the etch rate stable. High concentrations of ammonium fluoride are used in BOE as the total fluoride ion content is nearly that of concentrated 49% HF, and the BOE etchants are considered to pose the same toxic hazards as 49% HF[81-84]. In our experiment, we used 6:1 BOE. The specification for product of 6:1 BOE gives the percentage of ammonium fluoride and hydrofluoric acid as 33.8-35.8% and 6.2-6.6%, respectively. The etching process largely depends on timing of the dissolution. The BOE process is based on the complexing reaction:

$$SiO_2 + 6HF \longrightarrow H_2SiF_6 + 2H_2O \qquad 2.\ 42$$

where H_2SiF_6 is soluble in water.

The dilute HF solution is used to happen this reaction after mixing with buffer NH_4HF. The BOE has been kept in the plastic container. The glass substrate has been prepared using masking technique. The masked glass slide was dipped in the BOE to exposed the unprotected area by masking. The etching rate of 6:1 is $900A^0$/min. The glass slide has been exposed to the BOE. After 55 minutes the thickness profile has been monitored using the Dektak profilometer. Lithography bay is used for BOE experiment. The thickness for 55min exposure in the dipped glass substrate has been found in 22-25micrometer. The thickness of ~5 micrometer has been found for 6 minutes.

2.8. Spectrophotometer

A spectrophotometer is an optical characterization system which can determine the transmittance, absorbance, and reflectance spectrum of a sample from 190 nm to 1700 nm wavelength. The spectrophotometer has two main parts; a spectrometer which can produce light of any desired wavelength and a photometer which can detect the intensity of any incident light of any specific wavelength. Figure 2.21 shows the schematic diagram of a spectrophotometer. The main components of a spectrophotometer are a light source, a monochromator, a sample holder, and a detector. The monochromator splits the light coming from the source into individual wavelength components, and allows a single wavelength of light at a time. Then the light of single wavelength passes through the sample and incidents on the detector [85]. The detector can detect the intensity of light transmitted through the sample and give corresponding electrical signal. The software installed in the

computer receives this voltage signal and gives a spectrum over wide wavelength range (e.g. 190nm -1900 nm).

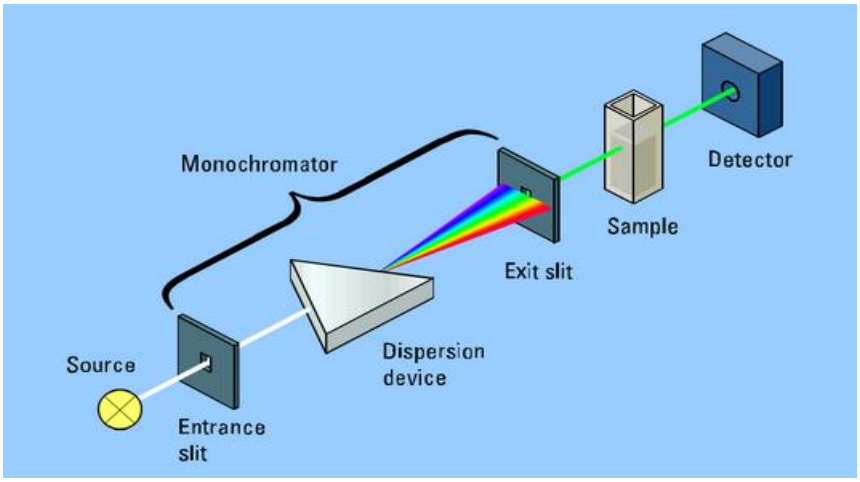

Figure 2. 20 Schematic diagram of spectrophotometer [86].

Transmittance is the ratio of transmittance irradiance (I) to incident irradiance (I_0) given in Eqn. 2.44 and usually expressed in percentage (%).

$$\%T = \frac{I}{I_0} \times 100 = 10^{-\alpha t} \times 100 \qquad 2.43$$

2.9. Contact Angle Measurer

One of the method of measuring the contamination level of the substrate is contact angle measurement. Contact angle is measured between the water droplet and substrate surface. If there is contamination in the substrate, then the water will form a droplet at the surface giving high contact angle as the contaminants repel the water and the water will adhere to itself forming a droplet and if there is no contamination then the water will spread out on the surface giving very little contact angle because water has high adhesion to clean glass substrate. Figure 2.22 shows the contact angle created by the water droplet on the substrate [87-89].

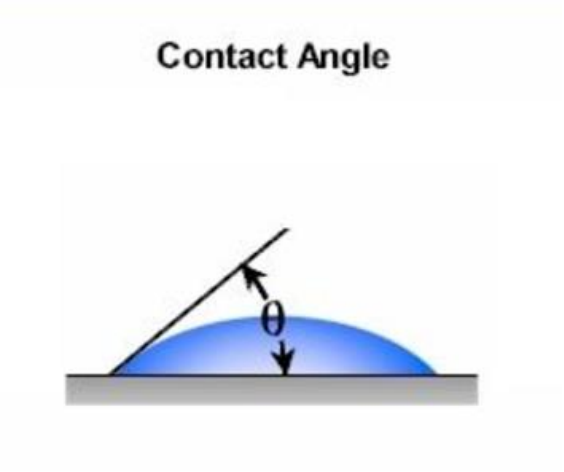

Figure 2. 21 Contact angle measurement system

2.10. SiO2 and Ag Properties

The reason of using the Ag layer in the proposed Fabry-Perot etalon structure rather than other metal is the highest reflectance (>90%) and lowest absorbance (<5%) than other metal (Al, Cu, Au, Cr) in the visible region from 400nm to 750nm [90] . Again Ag has some noble properties such as it has low refractive index, low loss which has great impact in the transmission of light through the Ag layer in the visible to near infrared region [91]. In the proposed modified Fabry-Perot Etalon, semitransparent layer of Ag is used to form the interference spectrum. As the Ag film thickness is too thin (about 10-15nm), light can pass through the Ag layer and the rest of the light will be reflected. The transmitted light has sufficient strength to pass through the second Ag layer. The transmitted light from second Ag layer will act as an output spectrum of the sensor from which the refractive index can be measured [92].

To create a cavity in the Fabry-Perot structure, a spacer is needed between two semitransparent layers. It is needed to change the medium or to flow the liquid of which

we want to measure the refractive index. In our proposed modified Fabry-Perot structure, Aluminum (Al) is used as the spacer layer. There is a significant impact of this spacer in the transmission spectrum. The output transmission spectrum contains more number of peaks of high transmission and becomes narrower when the cavity becomes wider and vice versa.

In the active layer, SiO_2 is used to increase the hydrophilicity of the surface so that liquid can easily flow into the cavity. The effect of SiO_2 on various surface has been investigated in many previous works [93-96]. Normally the Ag surface is not so hydrophilic because of the rough surface of the Ag layer deposited by physical vapor deposition. This will limit the scope of using the Fabry-Perot as a refractive index measuring technique of any liquid. To increase the easiness of the liquid flow in the active layer, the thin film of SiO_2 is used. It has been observed that the liquid spread in the surface so easily.

CHAPTER 3. EXPERIMENTAL PROCEDURE

3.1. Fabrication of Sensor

3.1.1. Making Hole in the Glass Slides Using EDM Process

To create an inlet and outlet port of microfluidic chamber, there is need of holes in the upper glass slide of the sensor. The glass slide was submerged in the electrolytic

solution of NaOH. Tungsten carbide (tungsten Carbide Round Rod, Ground, Precision Tolerance, ASTM B777-07, 0.3125" Diameter, 12" Length) was used as counter electrode and stainless steel (needle of a syringe) was used as tool electrode. The applied voltage was 50 volts and the current was 50 mA. The constant voltage mode was used during the electro machining process.

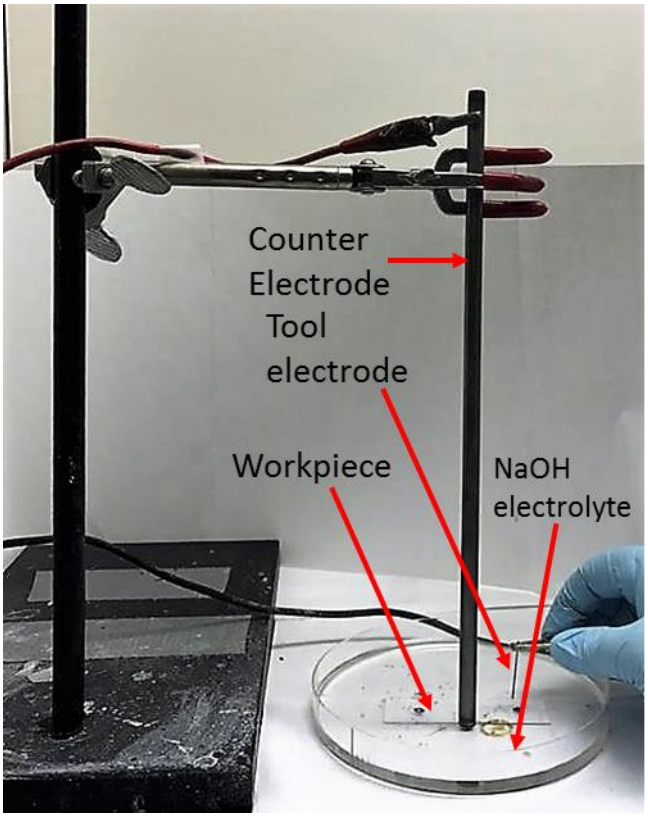

Figure 3. 1 Process of making hole in glass slides

3.1.2. **Substrate Preparation**

Glass microscope slides (Fisherbrand, Economy Plain) were cut into 1.5×1.0 inch^2 substrates for device fabrication. These substrates were soaked in a warm soap solution for 10 minutes to clean off the oils and organic residue. Then the glass substrates were soaked in DI water for 10 minutes. The substrates were then rinsed with the DI water several times

followed by ultra-sonication in fresh DI water. The glass substrates were then soaked in acetone for 10 minutes followed by ultra-sonication for 30 minutes. Likewise, the substrates were soaked in isopropanol for 10 minutes followed by ultra-sonication in isopropanol for 30 minutes. The glass substrates were then dried using nitrogen blow prior to silver deposition.

3.1.3. **Deposition of thin film**

Ag thin films were deposited on the glass substrates using a custom-built RF sputtering system with load-lock chamber. The conditions for the RF sputtering were: base pressure $1\text{-}2\times10^{-6}$ Torr, Ar gas flow 10 sccm, working pressure 3×10^{-3} Torr, RF power 50 W, reflection power 0 W, and deposition time 20 sec. Pre-sputtering of Ag was performed to avoid contamination from the target.

The Ag deposited glass substrates were masked in a hexagonal shape at the center to protect the active area from Al deposition. The Al spacer layer was deposited using the load-lock RF sputtering system. The base pressure for deposition was $1\text{-}2\times10^{-6}$ Torr. The Ag coated substrates were heated for 10 minutes at 150 $^{\circ}$C for better film adhesion prior to sputtering. The working pressure during the deposition was 4 mTorr. The applied RF power and Ar gas flow rate were 75 W and 10 sccm, respectively. The deposition produced Al spacers with thickness of 3-5 μm.

The SiO_2 thin films was sputtered on top of the Ag-coated glass substrates. The deposition conditions were: RF power 50 W, Ar gas flow rate 10 sccm, pressure 4 mTorr, and deposition time 3 min. The thickness of the SiO_2 layer was ~5 nm, which was deduced from a much longer deposition (e.g. two hours) using the same parameters.

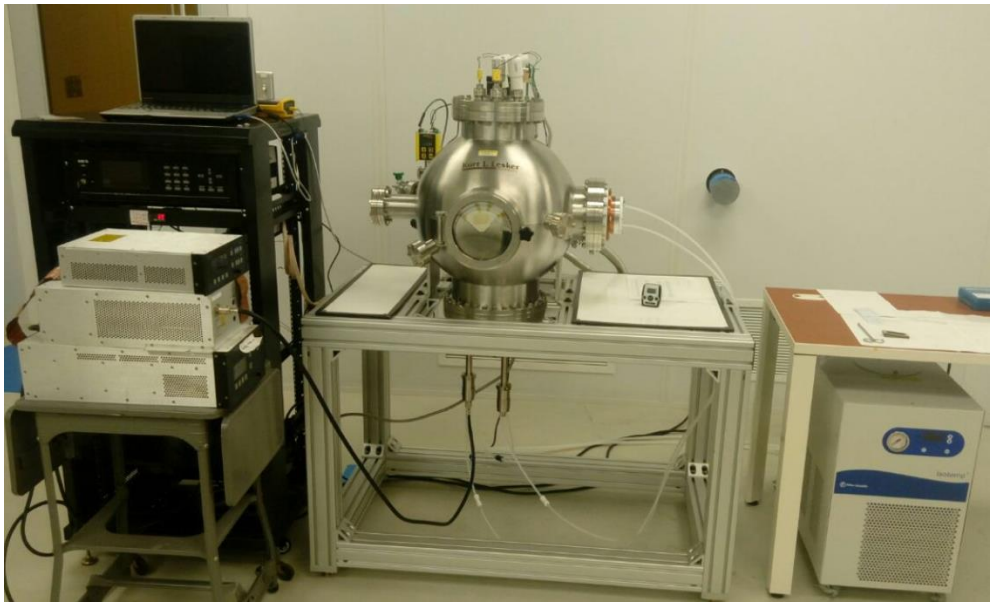

Figure 3. 2 Schematic view of Sputtering system

3.2. Characterization of the Sensor

3.2.1. Transmittance of Fabricated Sensor

Optical transmittance of the Fabry Perot Etalon sensors was measured using Filmetrics F-20 spectrometer thin film analyzer (thickness range 1nm-250nm and wavelength range 190 nm-1700 nm) with Hamamatsu (L120290) light source as shown in Figure 3.3 having combination of regulated and tungsten-halogen lamps. The light source was turned ON and the wait time of 5 minutes was maintained to let the light source be stable. Shutter of the source was opened to allow the light be incident on the sensors. Filmetrics F-20 software was used to investigate the spectrum. Optics recipe was edited for transmittance measurement. The system was calibrated for 100% and 0% transmittance by removing any

sample on the stage and placing an opaque sample on the stage respectively. Then the interested sample was placed on the stage, measurement was taken from the software.

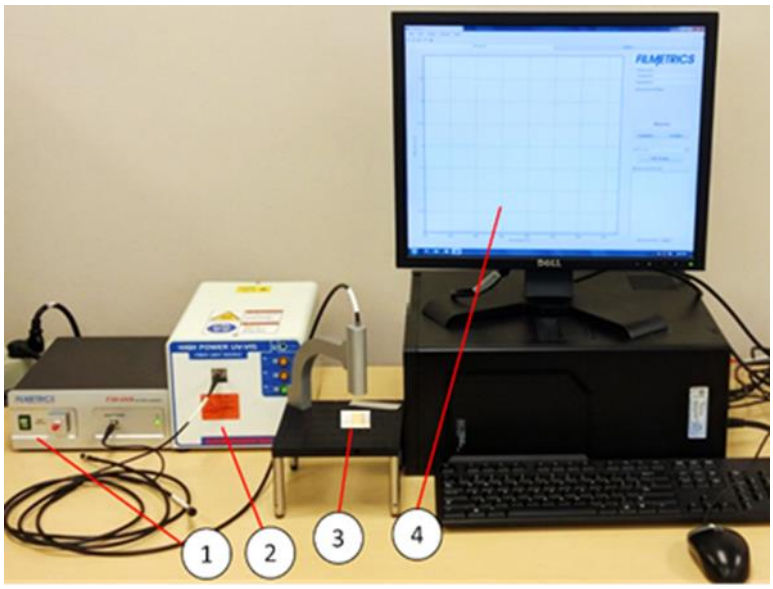

Figure 3. 3 Transmittance measurement system using Filmetrics F-20 optical spectrometer: (1) Light source combination of halogen and deuterium lamps (190nm-1700nm); (2) Thin film analyzer; (3) Fabry Perot Etalon sensor; (4) Filmetrics F-20 software.

3.2.2. **Hydrophilicity Test of Thin Film Through Contact Angle Measurement**

After turning on the Contact Angle Measurer, light source and computer, the sample is placed in the designated place in front of the camera. If the syringe is out of water, the DI water is used to fill the syringe by unscrewing the pin which holds in the syringe and pull out the syringe to remove the plunger and needle. By using the contact angle program to measure the contact angle, the hydrophilicity can be measured.

Figure 3. 4 Contact angle measurer

3.3. Biological Detection Using Fabry-Perot Etalon Sensor

The liquid was injected in the microfluidic chamber using the syringe infusion pump. Syringe infusion pump facilitates the liquid injection so that we can change the liquid solution easily one after another not interrupting the position of the sensor. Because it was observed that, the spectrum changed with the position where the light was pointing. After injecting the liquid in the microfluidic chamber, it was made sure the cavity is filled. When the liquid came out from the outlet port, then the transmittance was measured. Figure 3.5 shows the process of filling the microfluidic chamber with the intended liquid solution and software for measuring the transmittance. The recipe of the software was set to measure the transmittance. Then the peak wavelength from the transmittance spectrum was noted to find out the refractive index of the liquid.

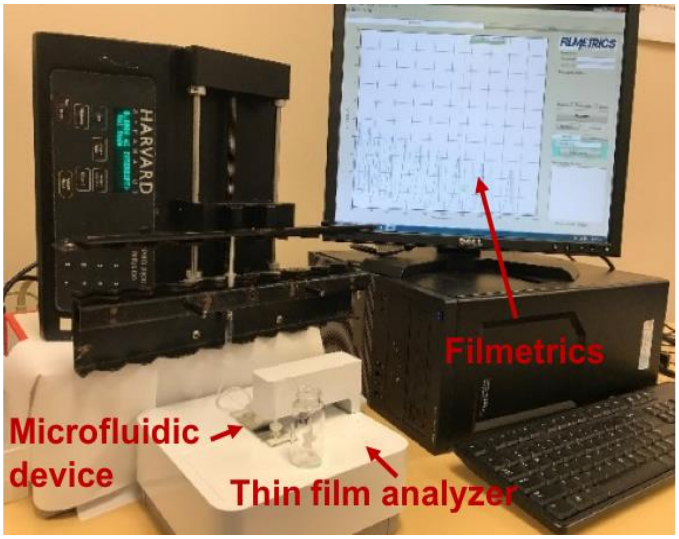

Figure 3. 5 Experimental setup with the syringe infusion pump, microfluidic sensor, spectrophotometer and software for analysis.

Figure 3.6 shows the optical set up where light source is a combination of regulated and tungsten-halogen lamps wavelength ranging from 190-1700nm. The transmitted spectrum was detected by spectrometer. Filmetrics F-20 software is used to make the detected spectrum visible for analysis.

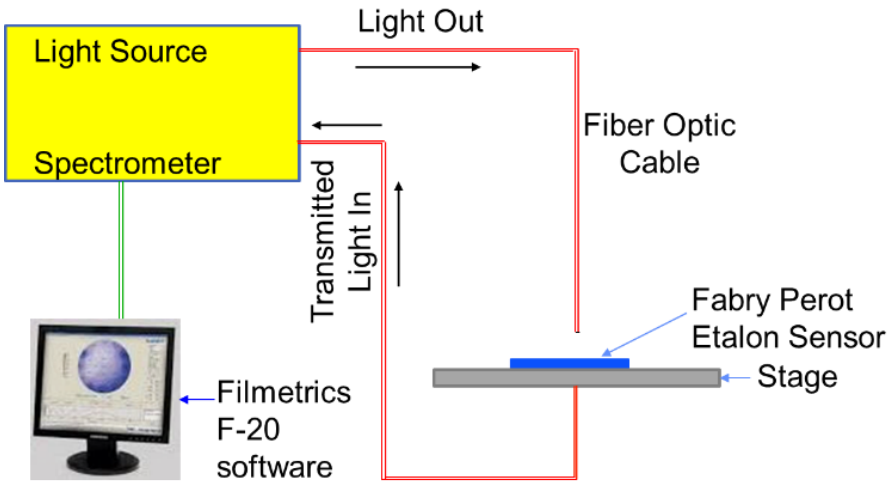

Figure 3. 6 Optical set up for biological substance detection

3.4. Sensor Structure

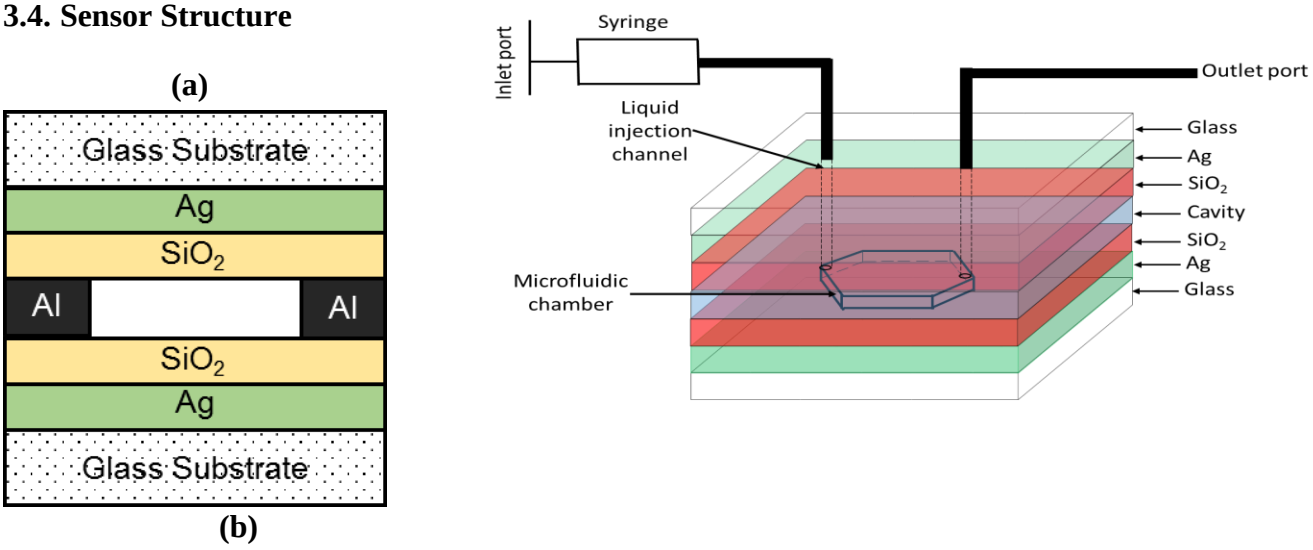

Figure 3. 7 An Enhanced Fabry-Perot etalon structure (a) 2D and (b) 3D

Figure 3.7 shows the sensor structure for the Fabry-Perot etalon proposed in this work. The top and bottom reflection layers were Ag thin films coated on glass slides. The Ag film thickness was about 10-15 nm, which led to very little absorption and allowed sufficient light to pass through the etalon and meanwhile created strong interference. A thin SiO_2 layer (~5 nm) was coated on the Ag films. It greatly increased the hydrophilicity of the surface so that the liquid could easily flow into the cavity. The SiO_2 film also protected the Ag film from oxidation and the sensor could be washed and reused. Since the SiO_2 layer was very thin, it had little effect on the optical characteristics of the Fabry-Perot sensor, as shown in the result section. An Al film was used as the spacer layer. Although any other films could be used as the spacer, the Al film could be used as electrodes for measuring electric properties in future tests. A larger space or thicker Al film will lead to

a transmission spectrum that has more and closer interference peaks according to equation 2.37.

CHAPTER 4. RESULTS AND ANALYSIS

4.1. Sensor Functionalization by Simulation and Wettability test

4.1.1. Simulation Result

The transmittance for liquid having different concentration were measured using the admittance method derived in the theory section. The shift of transmission peaks is clearly visible for different values of refractive index. The air spectrum can remain fixed for the convenience of calculation and show real time shift of peaks due to change of the concentration of any liquid. We choose some reference refractive index of glucose, NaCl and KCl from the work that has been done earlier. For the simulation, the Ag and SiO_2 thickness were assumed 15 nm and 5 nm respectively. The refractive index is a complex quantity having index and extinction co efficient. The value of refractive index has been chosen at ~589.00 nm wavelength. Dispersion effect was not taken into consideration as in the visible range there will be negligible change of refractive index value. The cavity thickness was 3μm and refractive index depends on the intended liquid. The parameter used for simulation are described in table 4.1

Reference Wavelength (nm): 589.00

Incident Angle (deg): 0.00

Table 4. 1 Parameter Simulation for transmittance spectrum of proposed enhanced Fabry-Perot etalon using admittance method

Layer	Material	Index of refraction	Extinction Co-efficient	Physical thickness
Medium	Glass	1.51674	0	
1	Ag	0.05890	3.65540	15nm
2	SiO2	1.45842	0.00000	5nm
3	Air	1	0	3um
	5% Glucose sol	1.338	0	3um
	10% Glucose sol	1.343	0	3um
	15% Glucose sol	1.348	0	3um
	20% Glucose sol	1.353	0	3um
	25% Glucose sol	1.358	0	3um
	5% NaCl sol	1.3418	0	3um
	10% NaCl sol	1.3505	0	3um
	15% NaCl sol	1.3594	0	3um
	20% NaCl sol	1.3684	0	3um
	25% NaCl sol	1.3778	0	3um
	5% KCl sol	1.33931	0	3um
	10% KCl sol	1.34643	0	3um
	15% KCl sol	1.35335	0	3um
	20% KCl sol	1.35992	0	3um
	25% KCl sol	1.3676	0	3um
4	SiO2	1.45842	0.00000	5nm
5	Ag	0.05890	3.65540	15nm
Substrate	Glass	1.51674	0	

Figure 4.1 shows the transmittance curve for air and different glucose solution. For real time measurement, the air spectrum should be fixed and the shift of peak wavelength for different liquid is measured. The spectrum shifted in one direction with the increasing of the refractive index of glucose solution from 1.338 to 1.358 or concentration of glucose solution from 5% to 25%.

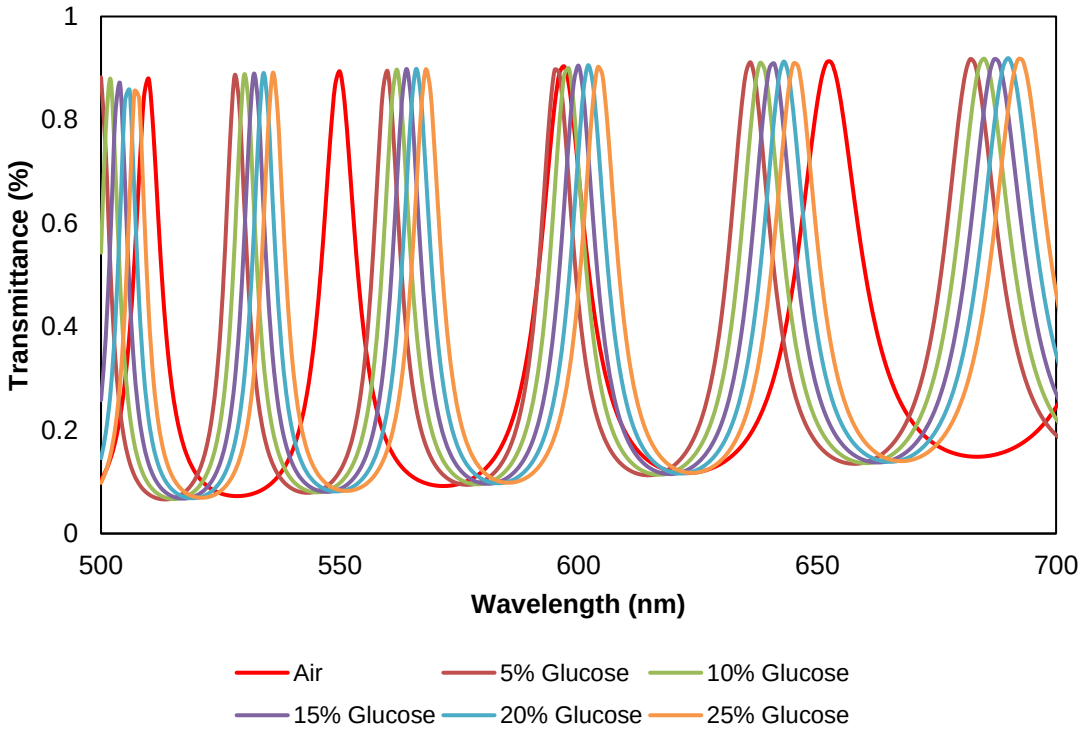

Figure 4. 1 Simulation of Transmission spectra of the Fabry-Perot etalons with air gap and Glucose-solution-filled gap. (a) 5% Glucose solution, (b) 10% Glucose solution, (c) 15% Glucose solution, (d) 20% Glucose solution, and (e) 25% Glucose solution.

Figure 4.2 shows the transmittance curve for air and different potassium chloride solution. For real time measurement, the air spectrum should be fixed and the shift of peak wavelength for different KCl is measured. The spectrum shifted in one direction with the increasing of the refractive index of KCl solution from 1.33931 to 1.3676 or concentration of KCl solution from 5% to 25%.

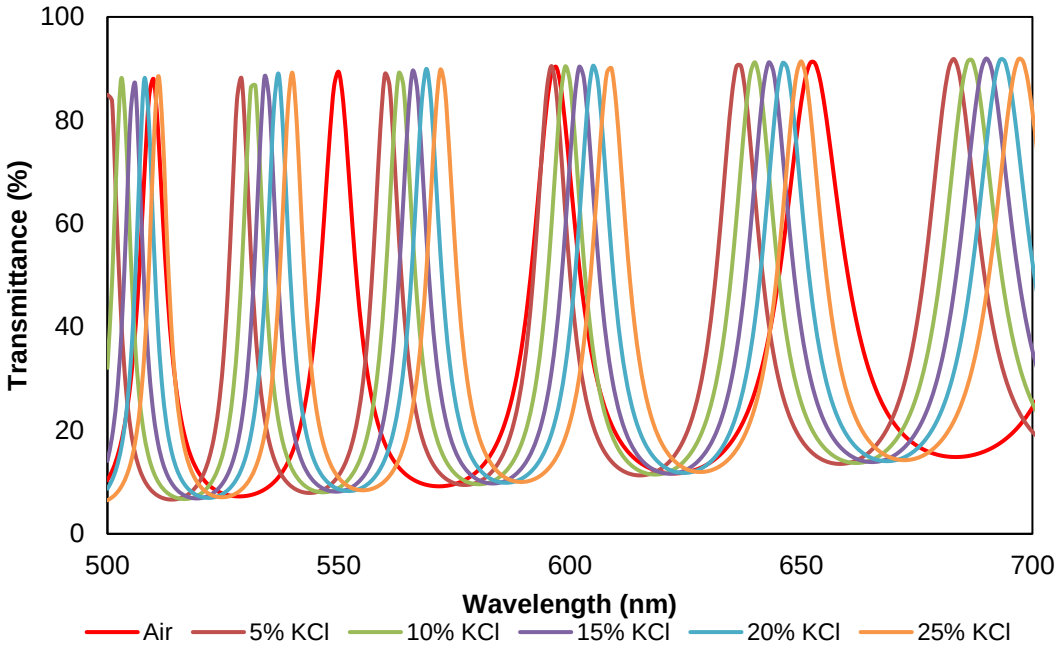

Figure 4. 2 Simulation of Transmission spectra of the Fabry-Perot etalons with air gap and KCl-solution-filled gap. (a) 5% KCl solution, (b) 10% KCl solution, (c) 15% KCl solution, (d) 20% KCl solution, and (e) 25% KCl solution.

Figure 4.3 shows the transmittance curve for air and different sodium chloride solution. For real time measurement, the air spectrum should be fixed and the shift of peak wavelength for different NaCl is measured. The spectrum shifted in one direction with the increasing of the refractive index of NaCl solution from 1.3418 to 1.3778 or concentration of NaCl solution from 5% to 25%.

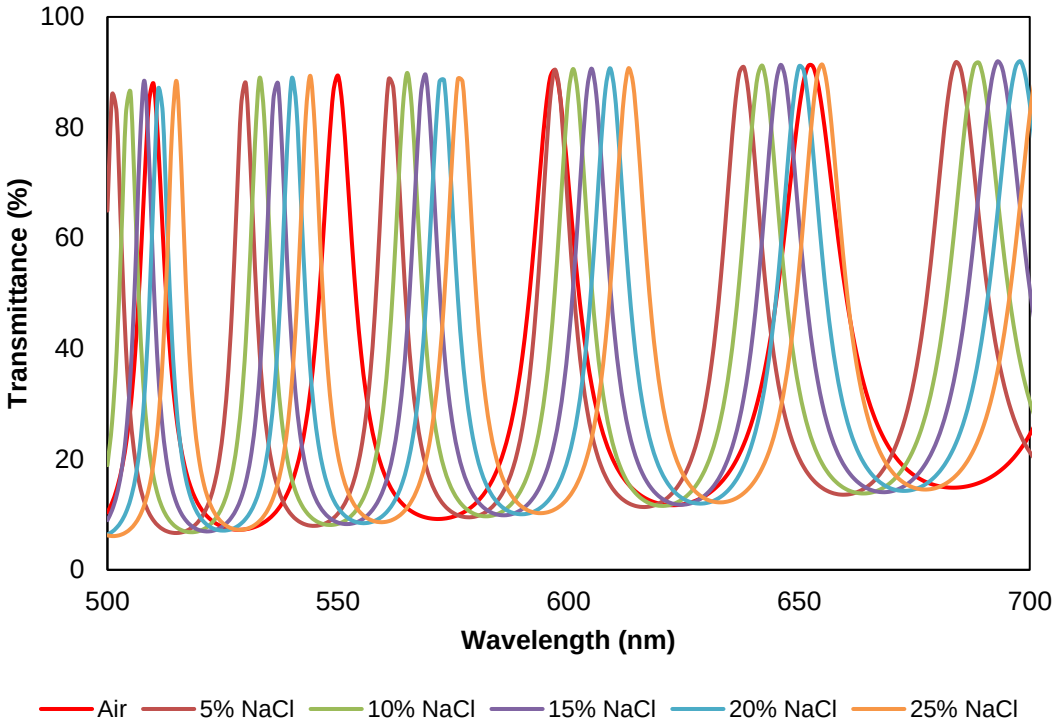

Figure 4. 3 Simulation of Transmission spectra of the Fabry-Perot etalons with air gap and NaCl-solution-filled gap. (a) 5% NaCl solution, (b) 10% NaCl solution, (c) 15% NaCl solution, (d) 20% NaCl solution, and (e) 25% NaCl solution.

The simulation result was verified with experimental as the medium of the cavity was changed and transmittance was measured each time light source pointing in the same position. The spectrum shifted per the concentration of the liquid. Figure 4.4 shows the real-time responses of the sensor for glucose, KCl and NaCl. The spectrum of glucose is narrower than KCl and NaCl while for NaCl the spectrum is wider, as the refractive index of glucose is low with compared to KCl and NaCl. The cavity was cleaned with DI water after measuring transmittance with one solution filled gap. When the spectrum back again in the air spectrum position then the next intended solution was injected. The transmittance

was measured when the cavity was filled. The measurement for other liquid solution was done in the same manner.

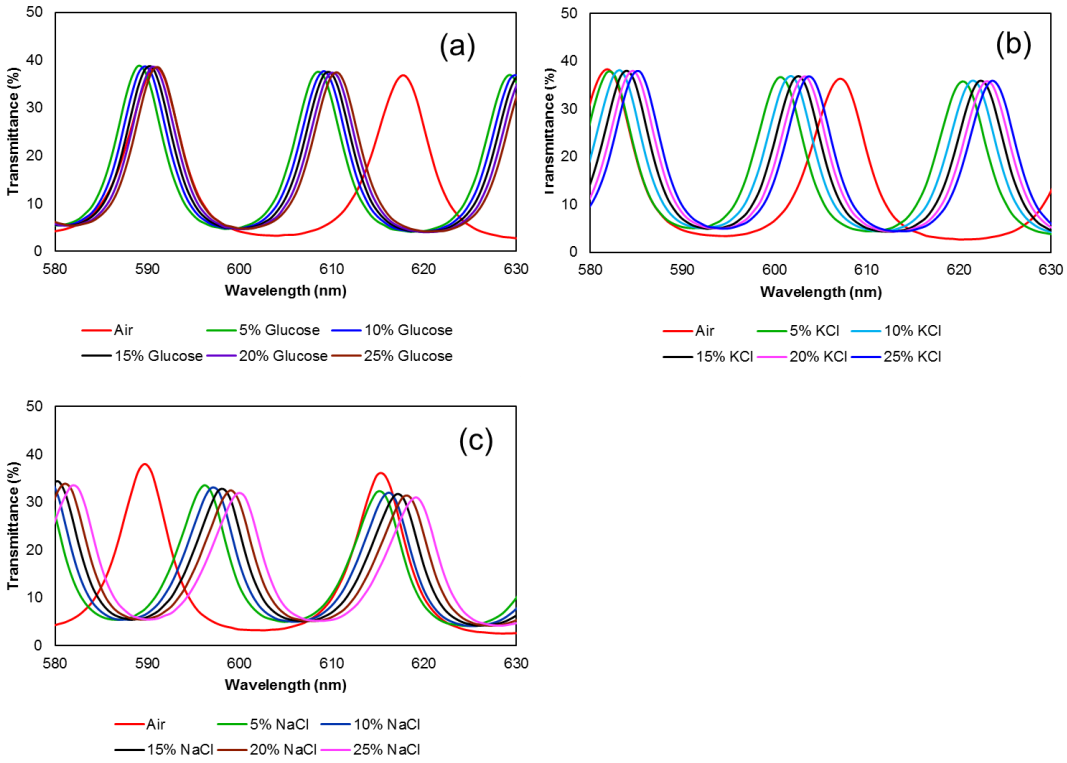

Figure 4. 4 Simulation of Transmission spectra of the Fabry-Perot etalons with air gap and solution-filled gap. (a) KCl solution, (b) Glucose solution, (c) NaCl solution

TABLE 4.2 summarizes the peak positions from the transmittance spectra of enhanced Fabry perot etalon, gap thickness and refractive index summary for different liquid solutions. With increasing wavelength, the separation of peak position increased for any liquid solution. The thickness of the cavity was found from the two peak wavelengths of air spectrum. As the thickness of the cavity doesn't change; the refractive index can be extracted using two peak wavelengths from the transmittance spectrum of

the liquid solution. With increasing the gap thickness, transmittance spectrum contains more peak wavelengths in the same wavelength range.

Table 4. 2 Summary of the peak positions in the transmission spectra with air gap and solution-filled gap, calculated gap thicknesses, and refractive indices.

Solution concentration (w/v%)	Air gap			Solution gap		
	Peak 1 (nm)	Peak 2 (nm)	Gap thick. (μm)	Peak 1 (nm)	Peak 2 (nm)	n
5% Glucose	591.17	617.79	6.859859397	588.99	608.51	1.338291186
10% Glucose	591.17	617.79	6.859859397	589.74	609.24	1.342978851
15% Glucose	591.17	617.79	6.859859397	590.2	609.65	1.348388276
20% Glucose	591.17	617.79	6.859859397	590.77	610.18	1.353647721
25% Glucose	591.17	617.79	6.859859397	591.18	610.55	1.358207543
5% KCl	581.80	607.09	6.983095334	581.98	600.67	1.339234825
10% KCl	581.80	607.09	6.983095334	583.2	601.87	1.34616386
15% KCl	581.80	607.09	6.983095334	583.9	602.51	1.353562752
20% KCl	581.80	607.09	6.983095334	584.65	603.21	1.360531333
25% KCl	581.80	607.09	6.983095334	585.29	603.8	1.367035608
5% NaCl	589.71	615.59	7.013515821	595.96	615.45	1.341628489
10% NaCl	589.71	615.59	7.013515821	596.99	616.41	1.350895422
15% NaCl	589.71	615.59	7.013515821	597.95	617.31	1.359242837
20% NaCl	589.71	615.59	7.013515821	599.14	618.44	1.368682773
25% NaCl	589.71	615.59	7.013515821	600.05	619.28	1.377619982

4.1.2. **Effect of SiO_2 in the Transmittance of Sensor**

Figure 4.5 shows the simulated transmittance spectra of a Fabry-Perot etalon illustrated in figure 3.7. The Ag film was 15 nm thick, the SiO_2 layer was 5 nm thick, and the air gap was 3 μm thick. The continuous line (green color) was the spectrum with 5 nm SiO_2 films and the dotted line (red color) was the spectrum with the SiO_2 films replaced with

equivalent air. This result confirmed that the peak shift induced by the thin SiO_2 layer was almost negligible.

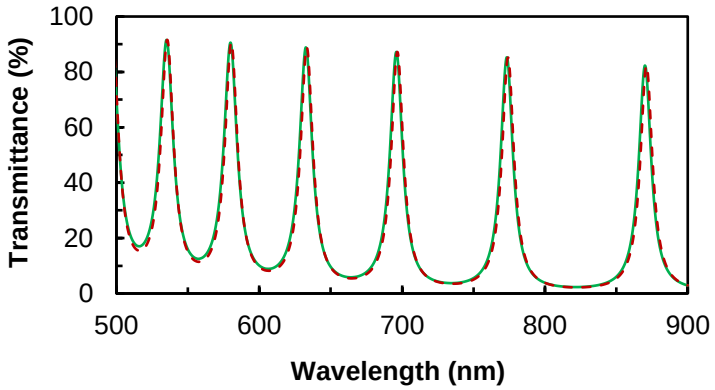

Figure 4. 5 Transmittance spectra of a modified Fabry-Perot etalon illustrated in FIG. 2.12. Continuous line (green): with SiO_2 thin layers of 5 nm thick. Dotted line (red): with the SiO_2 layers replaced with equivalent air.

4.1.3. **Surface Wettability Test**

The surface wettability of the Ag-coated glass substrates was evaluated using a contact angle measurement. Figure 4.6 indicated a hydrophobic surface of the Ag layer. The left and right contact angle of the Ag surface was 104^o and 103^o, respectively, which didn't allow liquid to flow easily in the Ag surface. With the SiO_2 layer on top of the Ag, the water drop spread out immediately and could not be measured. The super-hydrophilic SiO_2 surface allowed the sugar solutions to completely fill the cavity between the two SiO_2/Ag coated slides spaced with the Al layer.

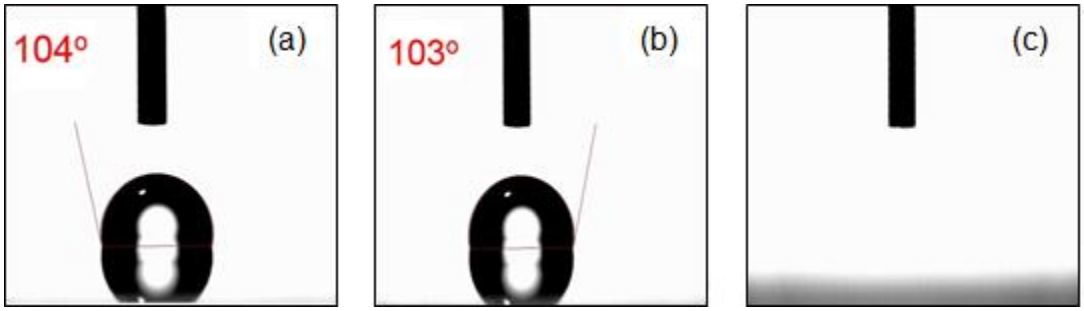

Figure 4. 6 Silver surface contact angles (a, b), and a completely wetted SiO_2 coated surface (c).

4.2. Refractive Index Measurement Procedure

The example of overall procedure of measuring the refractive index of a liquid solution is described using the 600 mg/dL glucose solution. The sensor was utilized for the measurement of refractive index of glucose, potassium, sugar and sodium solution of different concentration at room temperature. The transmittance spectrum of liquid was measured with the reference of air spectrum for finding the refractive index. As for example, detection of liquid (600mg/dL) using refractive index at ~590 nm is shown in figure 4.7. The peak wavelength of 572.09 nm and 616.28 nm was found for finding the gap thickness of 3.98 μm using air gap spectrum (n=1 known). The refractive index was found 1.3336 using the peak wavelength of 587.21 nm and 621.51 nm from the shift of spectrum for 600 mg/dL glucose solution. Same procedure was followed for other measurement of biological substances. The amount of analyte/biological substances for an unknown solution can be detected from the corresponding refractive index value from the linear response found after calibration.

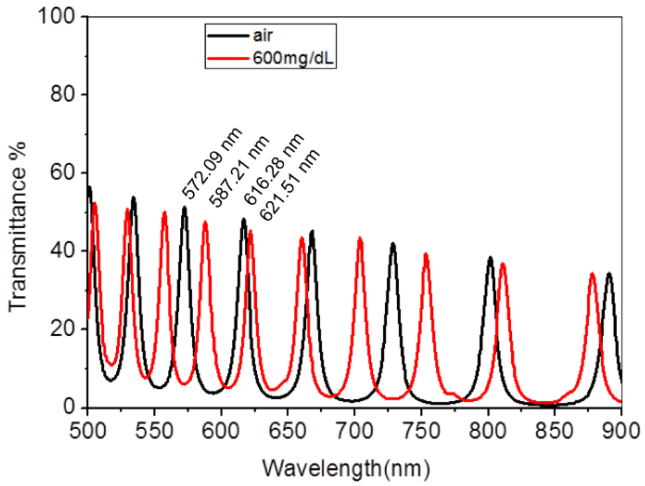

Figure 4. 7 Transmission spectra of the Fabry-Perot etalons with air gap and 600mg/dL glucose-solution-filled gap.

4.3. Detection of Sugar in DI water

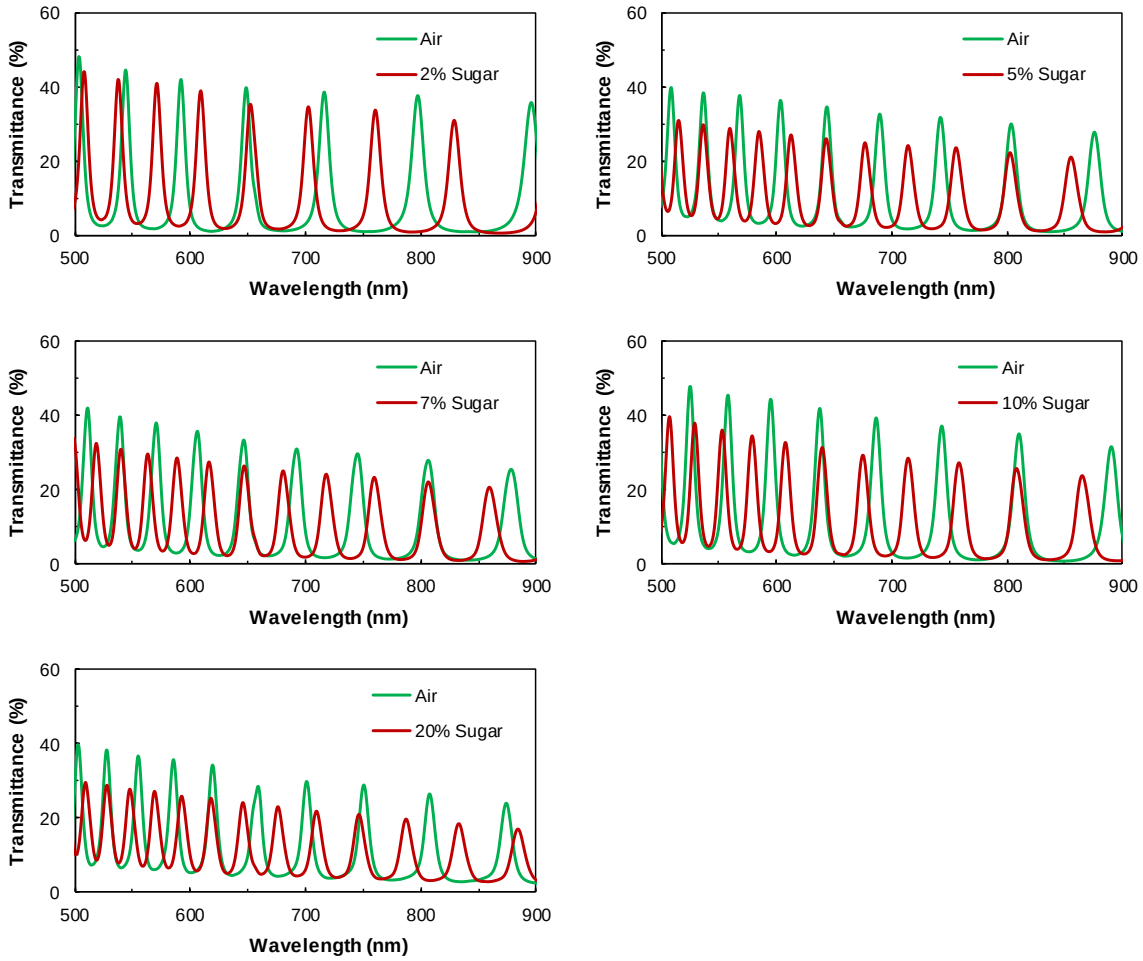

Figure 4. 8 Transmission spectra of the Fabry-Perot etalons with air gap and sugar-solution-filled gap. (a) 2% sugar solution, (b) 5% sugar solution, (c) 7% sugar solution, (d) 10% sugar solution, and (e) 20% sugar solution.

Sugar solutions with brix concentration from 2% to 20% were measured. Each solution was measured using a different sensor to ensure no cross-contamination. The transmission spectra with air and a sugar solution in the gap were measured and used to determine the gap thickness and the refractive index of the liquid, respectively. First, using two consecutive interference peaks with an air gap (refractive index 1.000), the gap thickness

was first determined. Using the gap thickness and two corresponding peaks in the transmission spectrum of a sugar solution, the refractive index of the liquid was subsequently calculated. The wavelength in which the refractive index was calculated was around 590 nm.

Figure 4.8 shows the wavelength shift due to change in the medium in the cavity. The cavity length has been found ~3.40 μm with the peak wavelength of 591.63 nm and 647.91 nm in the air medium. The refractive index of 2% sugar solution was calculated from two consecutive peak wavelengths. The refractive index of 1.337 has been found for 2% sugar solution with the peak wavelength of 570.70 nm and 608.84 nm. The wavelength and velocity of electromagnetic wave change when light travel in a medium other than air. For example; when light passes through the air medium, then the wavelength is λ. But in other medium, wavelength changes to λ/n as well as velocity changes to c/n from *c,* where *n* is the refractive index of medium. Depending on the medium refractive index, the wavelength changes accordingly.

As shown in figure 4.8, for 5% sugar solution, the wavelength for highest transmittance was 585.12 nm and 613.02 nm whereas for air medium it was 568.37 nm and 604.19 nm with ~590 nm reference wavelength. The length of the cavity was 4.79 μm. The refractive index of 1.341 was calculated for 5% sugar solution. The speed of light slows down and the wavelength got reduced in the medium having higher refractive index greater than 1. As the cavity length increased to 4.79 μm from 3.4 μm, the wavelength shortens and more peaks are available in the spectrum.

As shown in figure 4.8, for 7% sugar solution, the length of cavity was 4.82 μm with the peak wavelength of 570.23 nm and 606.05 nm in the air medium with reference wavelength of ~590 nm. The refractive index of 1.344 was calculated for 7% sugar solution with the peak wavelength of 587.91 nm and 615.81 nm. The intensity and half power band width both reduces at higher wavelength, which is attributed to absorbing medium.

Figure 4.8 Shows transmittance spectra for air medium, 10% sugar solution, and 20% sugar solution. Light needs to pass more path in sensor for 20% sugar solution than sensor for 10% sugar solution. That's why sensor for 20% sugar contains more peak wavelength than sensor for 10% sugar. In case of 10% sugar solution, light needs to pass through 4.52 μm with the peak wavelength of 558.6 nm and 595.35 nm in the air medium. The refractive index of 1.350 was calculated for 10% sugar solution with the peak wavelength of 579.53 nm and 608.37 nm. Similarly, for 20% sugar solution as shown in figure 4.8, the cavity length was 5.33 μm with the peak wavelength of 585.12 nm and 619.07 nm from the air medium. The refractive index of 1.365 was calculated for 20% sugar solution with the peak wavelength of 592.08 nm and 617.17 nm.

As the thickness of the cavity increases, light needs to travel longer propagation path in film and wave spends longer time in film. With increasing the extinction of wave, the absorption by material will also be increased. The transmittance has been reduced from ~42% to ~28% at 500nm for sugar solution as the length of the cavity increased from ~3.4 μm to 5.33 μm as shown in figure 4.8. This is true for other wavelengths also. The photon interacts with the atom of each layer of the sensor. The optical Refraction and absorption

occurs due to the interaction of photon with the electron of silver layer. The energy of photon will be absorbed for high index dielectric materials (SiO2) at longer wavelengths.

As an example, figure 4.8 shows the transmission spectra of a sensor with an air gap and 2% sugar solution, respectively. With an air gap, two consecutive interference peaks were found at 591.63 nm and 647.91 nm, which led to a gap thickness of 3.40 μm. With the 2% sugar filling in the gap, two interference peaks were found at 570.70 nm and 608.84 nm, from which the refractive index was deduced to be 1.337.

The transmission spectra of the 5%, 7%, 10%, and 20% solutions are shown in figure 4.8 each being measured with an air gap and a sugar-solution-filled gap, respectively. The gap thickness and refractive indices of the sugar solutions were determined in a similar way as the 2% sugar solution discussed above. Table 4.3 summarizes the peak positions, calculated gap thickness, and refractive indices.

Table 4. 3 Summary of the peak positions in the transmission spectra with air gap and sugar-solution-filled gap, calculated gap thicknesses, and refractive indices.

Sugar solution	Air gap			Solution gap		
	Peak 1 (nm)	Peak 2 (nm)	Gap thick. (μm)	Peak 1 (nm)	Peak 2 (nm)	n
2%	591.63	647.91	3.40	570.70	608.84	1.337
5%	568.37	604.19	4.79	585.12	613.02	1.341
7%	570.23	606.05	4.82	587.91	615.81	1.344
10%	558.60	595.35	4.52	579.53	608.37	1.350
20%	585.12	619.07	5.33	592.08	617.17	1.365

The refractive index vs. the brix concentration was plotted in Fig. 4.9, which shows a linear response. Using this linear relationship, the sugar concentration in water solution can be extracted from the value of refractive index. For an unknown sugar solution, after measuring the refractive index using this Fabry-Perot etalon, the brix percentage can be readily derived from the fitting equation given in figure 4.9. The sensitivity of this measurement is reflected by the slope of the linear fitting, being 1.7×10^{-3} refractive index per brix%. This sensitivity can be translated into wavelength difference using equation 2.37. Assuming the center wavelength between the two transmission peaks is 600 nm and the sensor has a gap of 500 nm thick, then a change of 1.7×10^{-3} in the refractive index will lead to a variation of 0.34 nm in the wavelength difference between the two transmission peaks. This variation in wavelength can be readily detected using a common spectrophotometer.

Although it is possible to detect any change of concentration by our proposed sensor theoretically. But in practical, the resolution or the proposed modified Fabry Perot Etalon sensor is ~0.05 brix%. Resolution is the smallest concentration difference that can be determined by the proposed sensor. It is a combination of sensor sensitivity and resolution (ΔR). It can be expressed as

$$\Delta C = \Delta R /(dn/dC)$$

From our experiment, we can detect the difference of refractive index up to third decimal. For example, we measured the refractive index of 1.3348 and 1.3331 for 1000mg/dL and 1200mg/dL glucose solution respectively. It is obvious from the refractive

index measurement of different liquid solution that our sensor can detect the change of RI easily up to fourth decimal. So, resolution of the proposed sensor is

$$\Delta C = \frac{.0001RI}{1.7*10^{-3}(\frac{RI}{Brix\%})} = .05 \text{ Brix\%}$$

As discussed before, the sensors measure the positions of the interference peaks. Therefore, the signal-to-noise ratio (SNR) depends on the resolution of the spectrophotometer. The maximum resolution of spectrophotometer in determining the peak wavelength is 0.1 Å or 0.01 nm. The uncertainty in the measurement of peak position in the interference spectrum will be considered as noise. This noise in determining the peak wavelength can be related to the uncertainty of the refractive index. The refractive index (n) of 1.337 was found for 2% sugar solution using the peak interference wavelength of transmittance spectrum given in Table I. The refractive index difference (Δn) of $4.5*10^{-5}$ was found due to the uncertainty in determining the peak positions from the transmittance spectrum. The SNR was found to be 54.69 dB, which was comparable or better than the other sensors available for detect the liquid/gas levels (50 dB in [97], 31.22 dB in [98] or 25 dB in [99]).

Table 4.4 compares our experimental results with the reported refractive indices of sugar solutions. They were in good agreement. Therefore, the Fabry-Perot etalon had excellent accuracy.

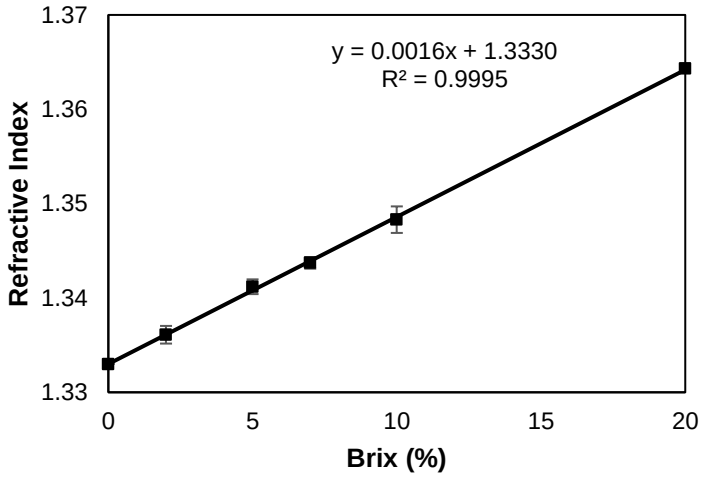

Figure 4. 9 Refractive index vs. brix (%) concentration. Circle: measured values. Continuous line: fitting result.

Table 4. 4 Comparison of the reported and experimental results.

Brix percentage	Refractive index reported	Refractive index measured(average)	Difference/measured ×100%
2	1.335	1.336	.07
5	1.340	1.341	.07
7	1.343	1.343	0
10	1.347	1.358	.81
20	1.363	1.364	.07

The refractive index of 5% sugar solution was measured at different temperature. The 5% sugar solution was heated to increase the temperature. Liquid was injected in the cavity after measuring the temperature by thermometer. The refractive index of liquid decreased with increasing temperature with a rate of .00014/^{o}C as liquid density decreased with increasing the temperature. The refractive index of 1.34, 1.338, 1.336 and 1.334 was found for 24.7^{0}C, 35.3^{0}C, 50.7^{0}C and 65.6^{0}C respectively with a reference wavelength of

~600nm. Thus, the refractive index is inversely proportional to temperature. The refractive index depends on the relative electric and magnetic susceptibility. The thermal collision between the electromagnetic wave and dielectric material will be increased with increasing temperature. The light needs more time to pass as it becomes hard for the dipole moments of the dielectric material to be aligned and medium susceptibility decreases with temperature. Figure 4.10 shows the transmittance (%) vs wavelength(nm) spectra for air and 5% solution filled gap at different temperature.

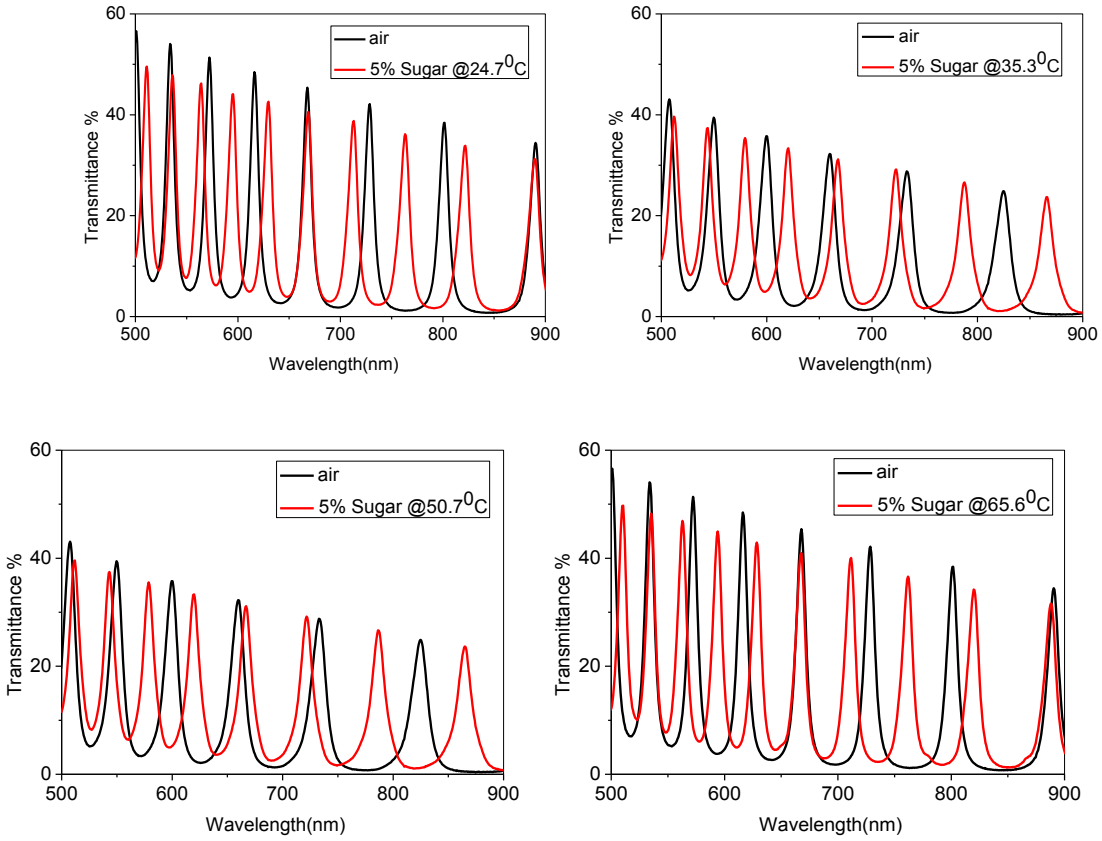

Figure 4. 10 Transmission spectra of the Fabry-Perot etalons with air gap and 5% sugar-solution-filled gap. (a) 24.7^0 C (b) 35.3^0 C, (c) 50.7^0 C, (d) 65.6^0 C

Table 4.5 summarizes the peak wavelength for air and 5% sugar solution filled gap at different temperature. The same point in the sensor was used for focusing light for 24.7 and 65.6^0 C as well as 35.3 and 50.7 ^{0} C. After injecting liquid, the transmittance was measured. The cavity was washed with the DI water to clean sugar particle from the cavity to use the same sensor more than once. The next solution was injected and transmittance was measured after cleaning properly when the transmittance spectrum came back to the previous position.

Table 4. 5 Summary of the peak positions in the transmission spectra with air gap and 5% sugar-solution-filled gap, calculated gap thicknesses, and refractive indices at different temperature.

Temperature (^{0}C)	Air gap			Solution gap		
	Peak 1 (nm)	Peak 2 (nm)	Gap thick. (μm)	Peak 1 (nm)	Peak 2 (nm)	n
24.7	572.09	616.28	3.99	563.95	595.35	1.340
35.3	550.00	600.00	3.30	579.65	620.35	1.338
50.7	550.00	600.00	3.30	579.07	619.77	1.336
65.6	572.09	616.28	3.99	562.79	594.19	1.334

Figure 4.11 shows the refractive index vs temperature (^{0} C) for 5% sugar solution. The refractive index decreases with the increase of temperature. Figure 4.9 shows the increase of refractive index with increase of concentration. As with increasing the temperature, the concentration decreases, the refractive index goes down with increasing temperature at a rate of .00014/^{o} C.

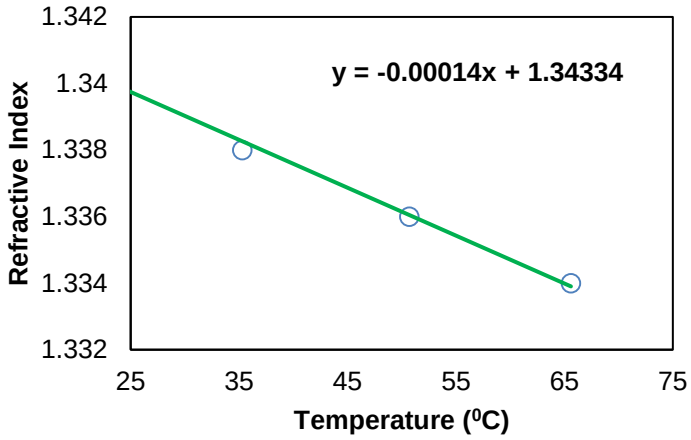

Figure 4. 11 Temperature effect on refractive index measurement for 5% sugar

4.4. Detection of Glucose in Water

Accurate detection of glucose is necessary for the diabetic patients. The glucose solutions were prepared adding glucose in DI water per the concentration as described earlier. The glucose level remains in diabetic patients from 200mg/dL to 700mg/dL. The detection of glucose at this small concentration needs highly sensitive and accurate sensor fabrication without any draw backs. The commercial glucose sensor purchased from *Freestyle Precision Neo* has error in the measurement of glucose concentration. The test of glucose solution having concentration of 20 mg/dL, 50 mg/dL, 100 mg/dL, 200 mg/dL and 500 mg/dL were performed. The commercial glucose level shows LO, 55 mg/dL, 126 mg/dL, 246 mg/dL and HI respectively for the above-mentioned glucose concentration solution. Each sensor can measure the refractive index more than once. But the fringe pattern changes after using several times and sometimes it loses its measuring ability. For the measurement of refractive index of many liquids several sensors were used. But is best to use different sensors for the measurement to avoid cross contamination.

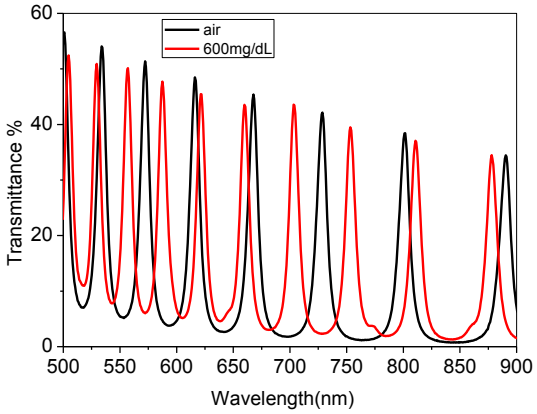
air
600mg/dL
Transmittance %
Wavelength(nm)

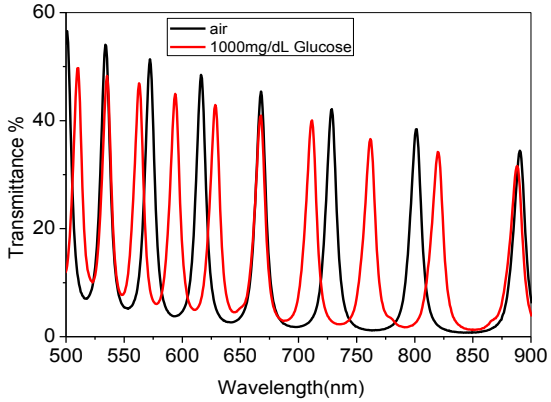
air
1000mg/dL Glucose
Transmittance %
Wavelength(nm)

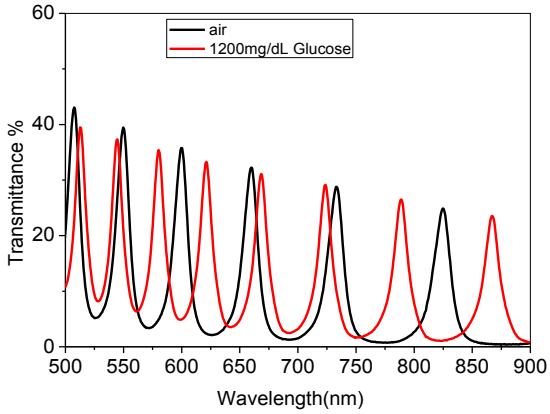
air
1200mg/dL Glucose
Transmittance %
Wavelength(nm)

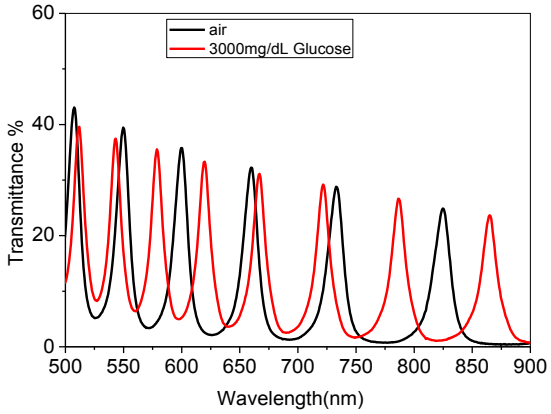
air
3000mg/dL Glucose
Transmittance %
Wavelength(nm)

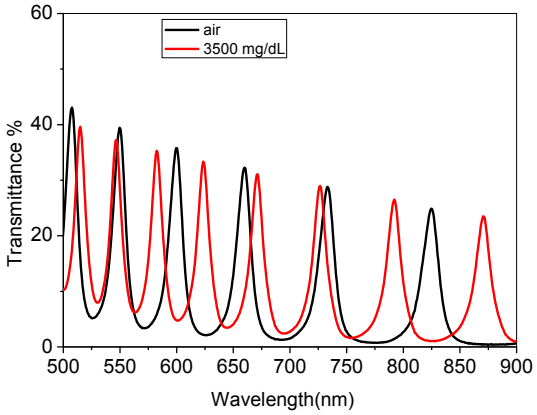
air
3500 mg/dL
Transmittance %
Wavelength(nm)

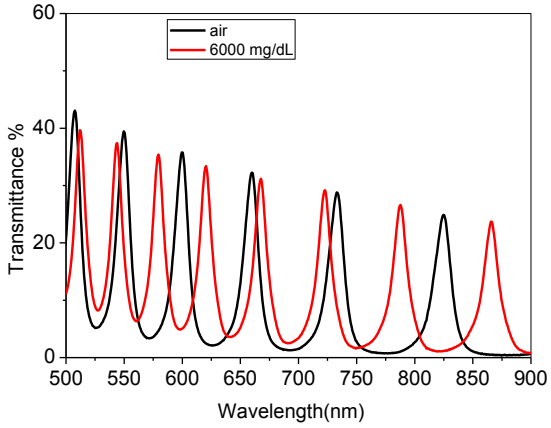
air
6000 mg/dL
Transmittance %
Wavelength(nm)

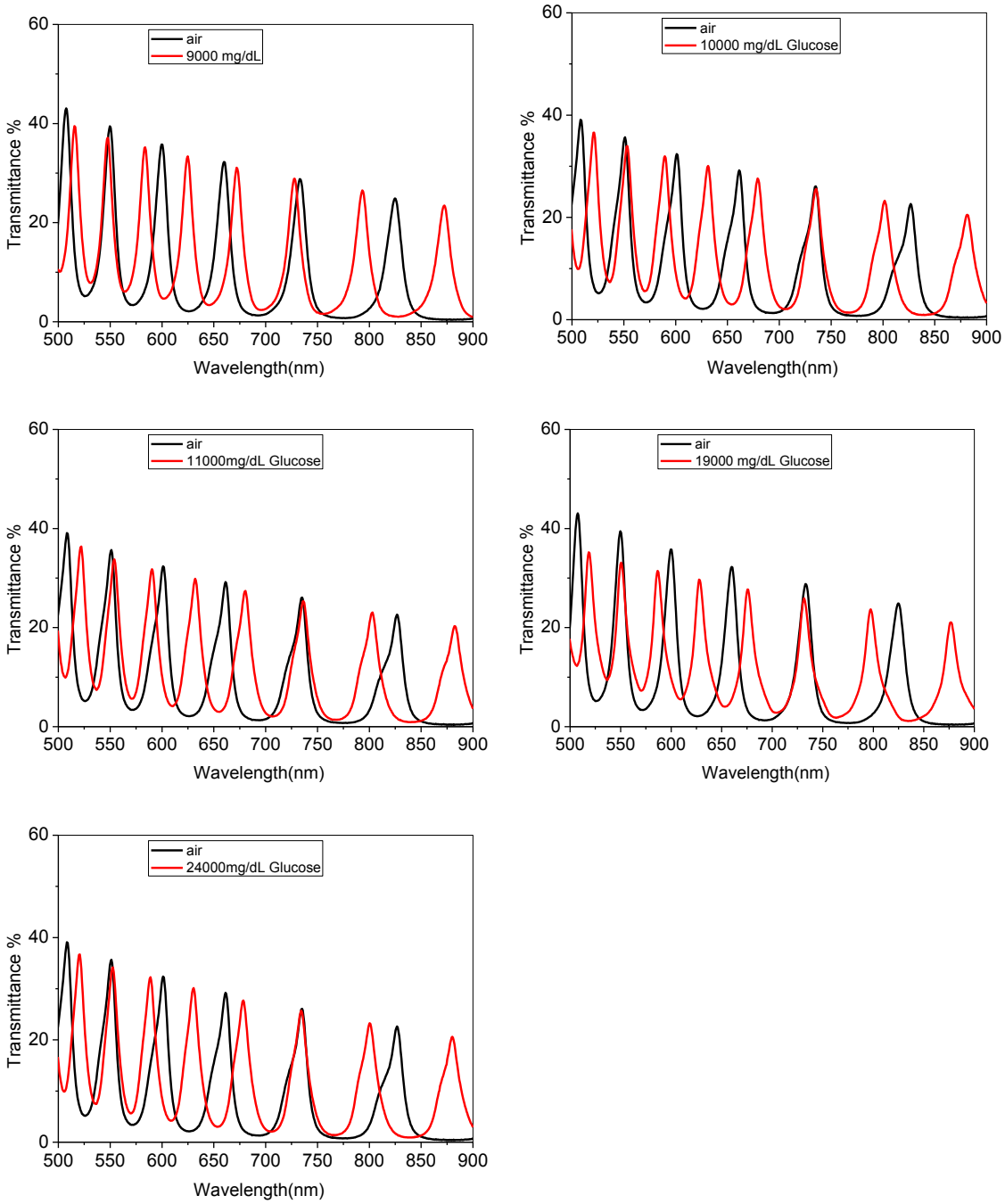

Figure 4. 12 Transmission spectra of the Fabry-Perot etalons with air gap and glucose-solution-filled gap

The detection of glucose solution up to 24% was performed. The injection of higher concentrated liquid in the cavity of micrometer thickness was not easy. The peak wavelength of air is used for finding the cavity thickness. We confined our measurement up to ~25% for any liquid detection.

The Table 4.6 summarizes the peak wavelengths for finding the cavity thickness from air spectrum. And, the peak wavelengths of the transmitted spectrum are also shown after using any liquid for finding the refractive index of the specified solution using the gap thickness calculated above.

Table 4. 6 Summary of the peak positions in the transmission spectra with air gap and glucose-solution-filled gap, calculated gap thicknesses, and refractive indices.

Glucose solution (mg/dL)	Air gap			Solution gap		
	Peak 1 (nm)	Peak 2 (nm)	Gap thick. (μm)	Peak 1 (nm)	Peak 2 (nm)	n
600	572.09	616.28	3.99	587.21	621.51	1.333610526
1000	572.09	616.28	3.99	562.79	594.19	1.334822854
1200	500.00	600	3.30	580.23	621.16	1.33419092
3000	500.00	600	3.30	579.07	619.77	1.336051723
3500	500.00	600	3.30	582.33	623.49	1.336531981
6000	500.00	600	3.30	579.65	620.35	1.338641492
6000_1	551.16	601.16	3.31	584.88	626.16	1.338796722
9000	500.00	600	3.30	583.72	624.88	1.342708991
10000	551.16	601.16	3.31	552.91	589.53	1.343211039
11000	551.16	601.16	3.31	590.12	631.98	1.344456272
17000	500.00	600	3.30	581.98	622.67	1.349380335
19000	500.00	600	3.30	586.63	627.91	1.352004211
24000	551.16	601.16	3.31	588.95	630.23	1.356875644

The refractive index of glucose solution increases with the concentration of glucose solution. The output spectrum from the sensor contains more number of peaks with the higher cavity thickness. It is clearly visible from the transmittance spectrum shown above in figure 4.13.

Glucose concentration for any unknown solution can be found using the calibration curve of refractive index vs glucose concentration. The plot of refractive index vs glucose concentration will give a linear equation. The refractive index of unknown glucose solution will be easily accessible from the linear equation also. The fitting with the actual data can be predicted from the R^2 value.

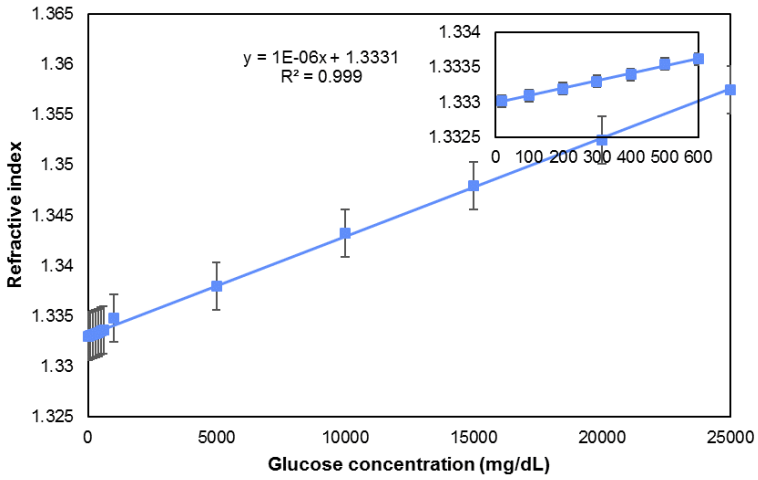

Figure 4. 13 Refractive index vs. solution concentration; Glucose at low concentration. cursor: measured values. Continuous line: fitting result.

The sensitivity of the glucose sensor has been found to be 10^{-6} RIU/mg/dL of glucose solution. The smallest unit of glucose solution that can be detected by the proposed sensor is 100 mg/dL. As compared with other types of liquid sensors, the sensitivity level is satisfactory. The linearity also proves the consistency of the sensor for getting accurate glucose level in liquid.

4.5. Detection of Potassium Chloride (KCl) in Water

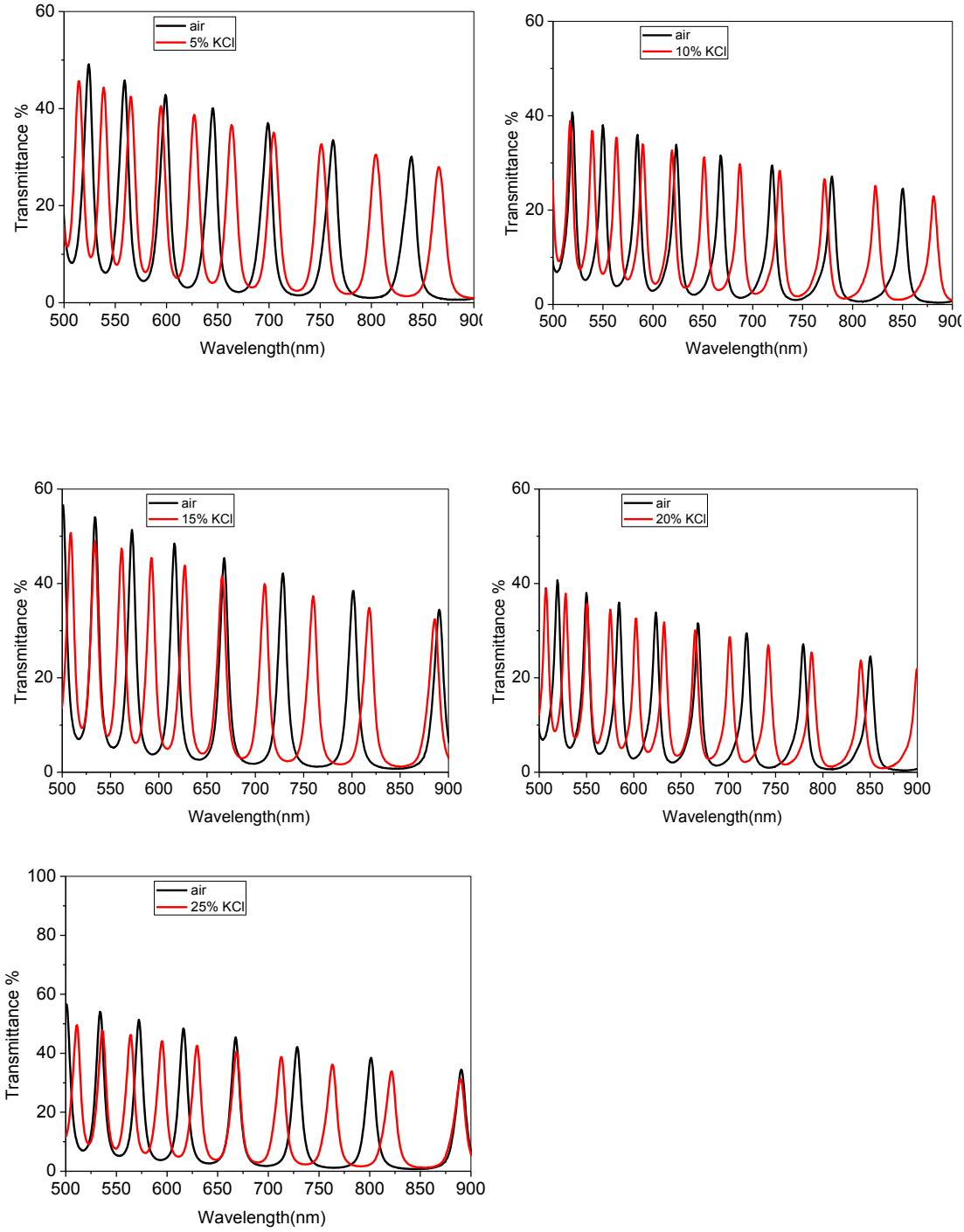

Figure 4. 14 Transmission spectra of the Fabry-Perot etalons with air gap and KCl-solution-filled gap

Figure 4.14 shows the wavelength shift due to a change of the medium in the cavity. The refractive index of 1.338 was found for the 5% KCl solution with the peak wavelength of 565.12nm and 594.77nm. As shown in figure 4.14, the transmittance peaks appeared at 590.12 nm and 619.19 nm for 10% KCl solution. The refractive index of 1.344 was calculated for 10% KCl solution. For 15% KCl solution, the refractive index of 1.353 was found with the peak wavelength of 561.63 nm and 592.44 nm which is shown in figure 4.14. Figure 4.14 shows transmittance spectra for air medium, 20% KCl solution, and 25% KCl solution. The refractive index of 1.355 was calculated for 20% KCl solution with the peak wavelength of 575 nm and 602.33 nm. Similarly, for 25% KCl solution as shown in figure 4.14, the refractive index of 1.364 was calculated with the peak wavelength of 563.95 nm and 594.77 nm. The different refractive index was found with different KCl solution containing different KCL level with the same water.

Figure 4.15 shows the transmittance vs wavelength of potassium chloride solution. For the glucose level measurement of diabetic patient, KCl detection will also be useful as blood contains KCl and other substances besides glucose. The transmittance vs wavelength spectrum get narrower with the increase of cavity gap thickness. For example, 10% KCL solution spectrum contains more number of peaks than 5% KCl solution as the cavity thickness is higher for 10% KCl solution. The transmittance intensities vary due to the thickness variation of silver layer. When the silver was deposited for 25 seconds using the condition mentioned in the experimental procedure, the transmittance intensities is about ~50%. But when the silver was deposited for 20 seconds, the intensities increased to ~60%. With increasing the thickness of the silver layer, the sharpness of the spectrum also

increases. The KCl has higher refractive index than glucose solution for the same concentration but less than sodium chloride.

Table 4.7 summarizes the peak wavelength of air spectrum and KCl solution filled gap wavelength for the transmittance spectrum. The gap thickness is found from the peak wavelength of air spectrum. The cavity thickness will remain unchanged, so we can use this gap thickness values for finding the refractive index of KCl solution.

Table 4. 7 Summary of the peak positions in the transmission spectra with air gap and KCl-solution-filled gap, calculated gap thicknesses, and refractive indices.

KCl solution	Air gap			Solution gap		
	Peak 1 (nm)	Peak 2 (nm)	Gap thick. (μm)	Peak 1 (nm)	Peak 2 (nm)	n
5%	559.3	598.84	4.235346636	565.12	594.77	1.338277199
10%	584.3	623.26	4.673650128	590.12	619.19	1.344723648
10%_1	551.16	601.16	3.313353456	586.63	627.91	1.346555372
15%	572.09	616.28	3.989224091	561.63	592.44	1.353581918
20%	584.3	623.26	4.673650128	575	602.33	1.355740325
25%	572.09	616.28	3.989224091	563.95	594.77	1.364076077
25%_1	551.16	601.16	3.313353456	558.14	594.77	1.367595053

The refractive index vs. % KCl solution shows a linear response with a sensitivity of $1.3*10^{-3}$ RIU per percent of KCl solution. The resolution of KCl detection is 0.07%. Using the linear response, the KCl content in KCl-water solution can be extracted from the value of refractive index. For any unknown KCl solution, after measuring the refractive index using the sensor, the percentage KCl content can be easily found from the following curve.

The refractive index of higher brix content sugar solution can be found by extrapolating the refractive index vs. % KCl solution response curve.

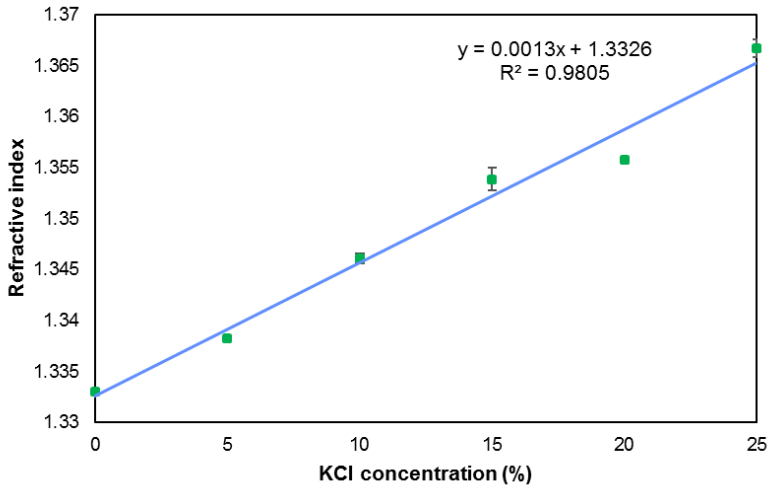

Figure 4. 15 Refractive index vs. solution concentration; KCl concentration. cursor: measured values. Continuous line: fitting result.

4.6. Detection of Sodium Chloride (NaCl) in Water

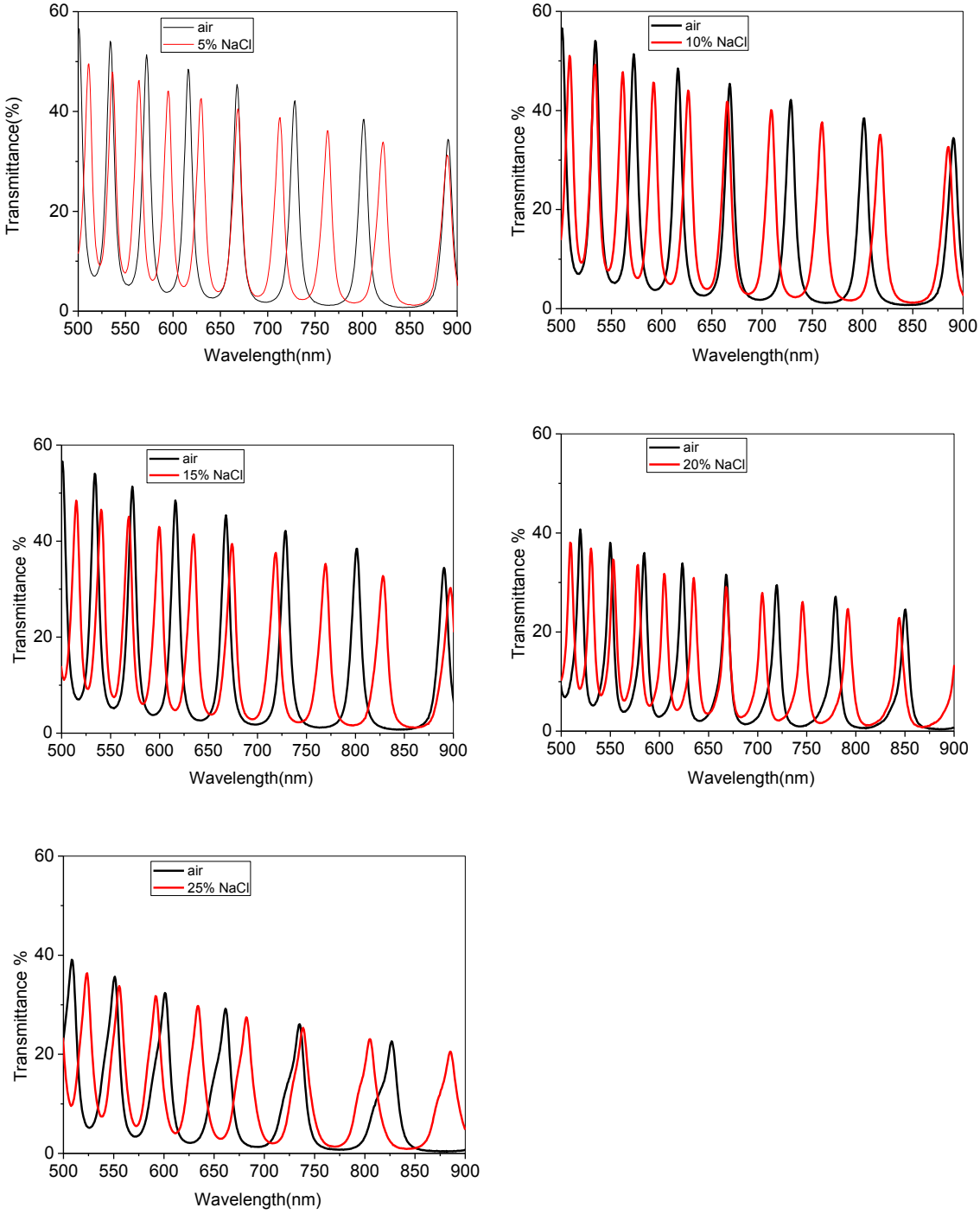

Figure 4. 16 Transmission spectra of the Fabry-Perot etalons with air gap and NaCl-solution-filled gap having concentration of 5%, 10%, 15%, 20% and 25%

Detection of NaCl was performed using the Fabry-Perot Etalon Based optical biosensor. NaCl detection is also important for the diabetic patient. As the blood contains sodium ion also. So, there is a potential of detecting the diabetic patient's condition through the measurement of Na^+ ion in blood. Figure 4.16 shows the transmittance vs wavelength spectrum for air and 5% to 25% NaCl solution filled gap.

Table 4.8 summarizes the parameter required to calculate the refractive index of NaCl solution and gap thickness for each measurement. The experiment was repeated for each solution to prove the repeatability.

Table 4. 8 Summary of the peak positions in the transmission spectra with air gap and NaCl-solution-filled gap, calculated gap thicknesses, and refractive indices.

NaCl solution	Air gap			Solution gap		
	Peak 1 (nm)	Peak 2 (nm)	Gap thick. (μm)	Peak 1 (nm)	Peak 2 (nm)	n
5%	572.09	616.28	3.989224091	563.95	595.35	1.340185399
5%_1	551.16	601.16	3.313353456	589.53	631.4	1.34155896
10%	572.09	616.28	3.989224091	561.05	591.86	1.350860272
10%_1	551.16	601.16	3.313353456	554.07	590.7	1.348332259
10%_2	558.14	608.72	3.358550621	562.21	599.42	1.348305268
15%	572.09	616.28	3.989224091	568.6	600	1.361789649
15%_1	551.16	601.16	3.313353456	556.4	593.02	1.359691426
20%	584.3	623.26	4.673650128	577.91	605.23	1.369663139
25%	551.16	601.16	3.313353456	555.81	591.86	1.377026551

The repeatability of this work is confirmed by the measurement of the NaCl solution for more than once. The slight deviation of each result proves the good agreement of the result with the theory with repeatability.

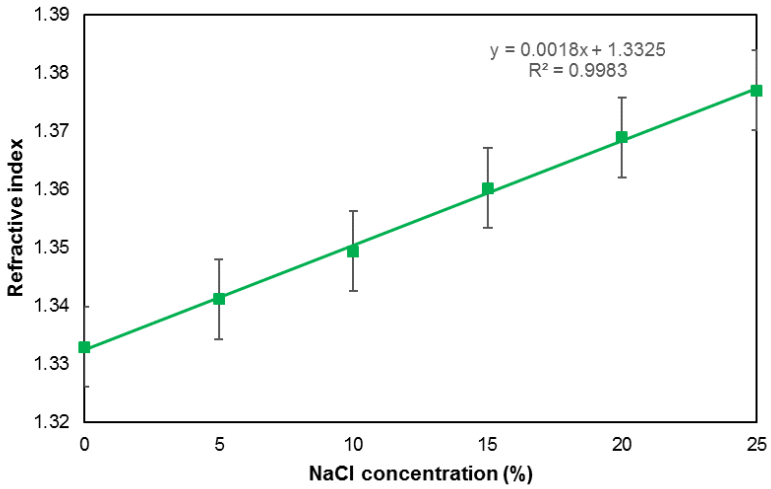

Figure 4. 17 Refractive index vs. solution concentration; NaCl concentration. cursor: measured values. Continuous line: fitting result.

The refractive index vs. % NaCl solution shows a linear response. From the linear response, the NaCl content can be extracted NaCl solution from the value of refractive index. For any unknown NaCl solution, after measuring the refractive index using the sensor, the percentage NaCl content can be easily found from the curve shown in FIG. 4.17. The sensitivity of the proposed sensor for NaCl detection was $1.8*10^{-3}$ RIU per percent of NaCl solution. The smallest change of NaCl solution that can be detected by the Fabry-Perot sensor is 0.5%.

CHAPTER 5. CONCLUSIONS

5.1. Summary

Fabry-Perot Etalon is an accurate approach to measure the refractive index of liquid. Fabry-Perot technique can increase the performance of optical sensor. As most of the Fabry-Perot sensors are based on optical fiber. The optical fiber based Fabry-Perot sensor has complex structure and costly optical set up. It is needed to find the Fabry-Perot Etalon based optical biosensor with simple structure and less expensive optical set up. The proposed optical sensor is the simplest design of the available liquid sensor. Again, the hydrophobic surface of active layer is a drawback of the proposed liquid sensor. It was not easy to flow the liquid in the cavity as the wettability of silver surface was poor. After the plasma treatment and different metal-oxide deposition, it was found that SiO_2 provides super hydrophilic surface without the need of any plasma treatment. The detection of sugar was performed using the proposed modified Fabry-Perot Etalon based sensor. The sensitivity for sugar detection was found $1.7*10^{-3}$ RIU per percent brix content with good linearity. The smallest concentration difference that can be determined by the proposed sensor is ~0.05 brix% which is comparable with the other approaches mentioned in [100, 101]. The resolution of the concentration was found from the sensitivity and resolution of the refractive index which is 10^{-4} RIU. Another important factor is temperature cross sensitivity. To get the accurate result, the temperature effect should also be considered. The refractive index decreases with the increase of temperature.

The sensor performance can be increased by incorporating microfluidic chamber with the modified Fabry-Perot Etalon based sensor. The microfluidic chamber with the inlet and outlet port helps to inject and take out the liquid easily and make sure that the

cavity is filled. This feature of the sensor helps to measure the liquid response accurately. The sensitivity for glucose, KCl and NaCl was found 10^{-6} RIU/ mg/dL, $1.3*10^{-3}$ RIU/% KCL and $1.8*10^{-3}$ RIU per percent of NaCl respectively.

Unfortunately, there is no direct approach to find the signal to noise ratio for our proposed sensor. The transmittance spectrum from our sensor contains some noise due to the imperfection of the thin film and impurity/defect in the cavity. The refractive index of hemoglobin can be determined by the proposed Enhanced Fabry-Perot Etalon sensor. Friebel and Meinke already showed it is possible to measure the glucose level from the refractive index measurement[102]. Mazarevica et al reported that high concentrations of glucose leads to an increase of the refractive index of hemoglobin in diabetic patients[103]. So, this sensor has the potential to measure the glucose level in blood samples of the diabetic patients. For real application, it needs some modification and high quality thin film with sophisticated fabrication process. The resolution needs to be improved for real application.

The result obtained from proposed sensor has been verified with the simulation using admittance method as well as from MacLeod software. The practical and theoretical result are in good agreement. The advantages of the proposed sensor are the accuracy, simple structure, less expensive set up, small size, less weight, the sensor is not corrosive and gives accurate result ignoring the effect of electromagnetic interference and mechanical disturbances. Another expected feature of this sensor is the reusability. The sensor can be used more than once for detecting the liquid solution. The cavity needs to be

cleaned with DI water to make sure there is no other substance available in the cavity to use the sensor more than once.

The response time is very short for the proposed Fabry-Perot etalon sensor for using the microfluidic structure with inlet and outlet port. Some other liquid sensor detection process is time consuming for filling the liquid in the cavity whereas some liquid sensor needs pumping to flow the liquid in the cavity. But our proposed sensor can detect liquid within a second after filling the cavity.

5.2. Conclusions

A microfluidic enhanced Fabry-Perot etalon using two semi-transparent Ag/SiO_2 surfaces is highly accurate in determining the refractive indices of sugar, glucose, KCl, NaCl solutions. The SiO2 film not only protects the reflective Ag layer, but also provides a super hydrophilic surface that allows liquid to easily flow into the cavity. The refractive index is linearly proportional to the liquid concentration. This sensor has the potential to accurately detect specific chemical species in liquids. This sensor will be the simplest sensor with high sensitivity and resolution with less expensive optical set up. The proposed sensor has the prospect of fulfilling the requirement of the Food and Drug Administrative (FDA) for the glucometer's accuracy as the current glucometer is not providing the accurate result. The detection of sugar, glucose, NaCl and KCl can be a base for the detection of glucose in blood for diabetic patients. The primary results prove that the sensor has some excellent features than some other liquid sensors and commercial glucometer.

5.3. Future work

The active layer of the sensor can be made more interactive to immobilize/ capture the biomolecule. The use of the capturing technique using antibody or modification of the active layer by some porous or photonic techniques will greatly enhance the sensor's performance. The detection of biomolecule or biological substances can be accurately detected by the proposed enhanced Fabry-Perot Etalon based microfluidic optical biosensor.

REFERENCES

1 Wei, T., Han, Y., Li, Y., Tsai, H.-L., and Xiao, H.: 'Temperature-insensitive miniaturized fiber inline Fabry-Perot interferometer for highly sensitive refractive index measurement', Optics Express, 2008, 16, (8), pp. 5764-5769

2 Ferreira, M.F., Statkiewicz-Barabach, G., Kowal, D., Mergo, P., Urbanczyk, W., and Frazão, O.: 'Fabry-Perot cavity based on polymer FBG as refractive index sensor', Optics Communications, 2017, 394, pp. 37-40

3 Domachuk, P., Littler, I., Cronin-Golomb, M., and Eggleton, B.: 'Compact resonant integrated microfluidic refractometer', Applied Physics Letters, 2006, 88, (9), pp. 093513

4 Fan, X., White, I.M., Shopova, S.I., Zhu, H., Suter, J.D., and Sun, Y.: 'Sensitive optical biosensors for unlabeled targets: A review', analytica chimica acta, 2008, 620, (1), pp. 8-26

5 Deng, M., Tang, C.-P., Zhu, T., Rao, Y.-J., Xu, L.-C., and Han, M.: 'Refractive index measurement using photonic crystal fiber-based Fabry-Perot interferometer', Applied optics, 2010, 49, (9), pp. 1593-1598

6 Liang, W., Huang, Y., Xu, Y., Lee, R.K., and Yariv, A.: 'Highly sensitive fiber Bragg grating refractive index sensors', Applied physics letters, 2005, 86, (15), pp. 151122

7 Ran, Z.L., Rao, Y.J., Liu, W.J., Liao, X., and Chiang, K.S.: 'Laser-micromachined Fabry-Perot optical fiber tip sensor for high-resolution temperature-independent measurement of refractive index', Optics express, 2008, 16, (3), pp. 2252-2263

8 Chen, M., Geiser, M., Truffer, F., and Song, C.: 'Development of interferometer for refractive index measurement of aqueous solution in a microfluidic chip', Laser Physics Letters, 2013, 10, (4), pp. 045701

9 Xue, L., Che, D., and Yang, L.: 'Liquid level sensing based on leaky mode attenuation in a guided-mode–leaky-mode–guided-mode fiber structure', Optics Communications, 2014, 325, pp. 160-164

10 Zhang, T., Pathak, P., Karandikar, S., Giorno, R., and Que, L.: 'A polymer nanostructured Fabry–Perot interferometer based biosensor', Biosensors and Bioelectronics, 2011, 30, (1), pp. 128-132

11 Homola, J.: 'Surface plasmon resonance sensors for detection of chemical and biological species', Chemical reviews, 2008, 108, (2), pp. 462-493

12 Homola, J.: 'Present and future of surface plasmon resonance biosensors', Analytical and bioanalytical chemistry, 2003, 377, (3), pp. 528-539

13 Homola, J., Yee, S.S., and Gauglitz, G.: 'Surface plasmon resonance sensors: review', Sensors and Actuators B: Chemical, 1999, 54, (1), pp. 3-15

14 Hoa, X., Kirk, A., and Tabrizian, M.: 'Towards integrated and sensitive surface plasmon resonance biosensors: a review of recent progress', Biosensors and Bioelectronics, 2007, 23, (2), pp. 151-160

15 Rothenhäusler, B., and Knoll, W.: 'Surface plasmon microscopy', 1988

16 Monzón-Hernández, D., and Villatoro, J.: 'High-resolution refractive index sensing by means of a multiple-peak surface plasmon resonance optical fiber sensor', Sensors and Actuators B: Chemical, 2006, 115, (1), pp. 227-231

17 Vo-Dinh, T., Yan, F., and Wabuyele, M.B.: 'Surface-enhanced Raman scattering for medical diagnostics and biological imaging', Journal of Raman Spectroscopy, 2005, 36, (6-7), pp. 640-647

18 Fleischmann, M., Hendra, P.J., and McQuillan, A.J.: 'Raman spectra of pyridine adsorbed at a silver electrode', Chemical Physics Letters, 1974, 26, (2), pp. 163-166

19 Tanahashi, I., Yamazaki, F., and Hamada, K.: 'Localized surface plasmon resonance sensing properties of Ag/TiO2 films', Chemistry Letters, 2006, 35, (4), pp. 454-455

20 Yu, F., Ahl, S., Caminade, A.-M., Majoral, J.-P., Knoll, W., and Erlebacher, J.: 'Simultaneous excitation of propagating and localized surface plasmon resonance in nanoporous gold membranes', Analytical Chemistry, 2006, 78, (20), pp. 7346-7350

21 Mayer, K.M., and Hafner, J.H.: 'Localized surface plasmon resonance sensors', Chemical reviews, 2011, 111, (6), pp. 3828-3857

22 Sai, V.V.R., Kundu, T., and Mukherji, S.: 'Novel U-bent fiber optic probe for localized surface plasmon resonance based biosensor', Biosensors and Bioelectronics, 2009, 24, (9), pp. 2804-2809

23 Bhatia, V., and Vengsarkar, A.M.: 'Optical fiber long-period grating sensors', Optics Letters, 1996, 21, (9), pp. 692-694

24 Patrick, H.J., Kersey, A.D., and Bucholtz, F.: 'Analysis of the response of long period fiber gratings to external index of refraction', Journal of lightwave technology, 1998, 16, (9), pp. 1606

25 White, I.M., Oveys, H., and Fan, X.: 'Liquid-core optical ring-resonator sensors', Optics letters, 2006, 31, (9), pp. 1319-1321

26 Sumetsky, M., Windeler, R.S., Dulashko, Y., and Fan, X.: 'Optical liquid ring resonator sensor', Optics Express, 2007, 15, (22), pp. 14376-14381

27 Fan, X., White, I.M., Zhu, H., Suter, J.D., and Oveys, H.: 'Overview of novel integrated optical ring resonator bio/chemical sensors', in Editor (Ed.)^(Eds.): 'Book Overview of novel integrated optical ring resonator bio/chemical sensors' (International Society for Optics and Photonics, edn.), pp. 64520M-64520M

28 Jágerská, J., Zhang, H., Diao, Z., Le Thomas, N., and Houdré, R.: 'Refractive index sensing with an air-slot photonic crystal nanocavity', Optics letters, 2010, 35, (15), pp. 2523-2525

29 Wu, D.K.C., Kuhlmey, B.T., and Eggleton, B.J.: 'Ultrasensitive photonic crystal fiber refractive index sensor', Optics letters, 2009, 34, (3), pp. 322-324

30 Chow, E., Grot, A., Mirkarimi, L.W., Sigalas, M., and Girolami, G.: 'Ultracompact biochemical sensor built with two-dimensional photonic crystal microcavity', Optics letters, 2004, 29, (10), pp. 1093-1095

31 Jiang, L., Yang, J., Wang, S., Li, B., and Wang, M.: 'Fiber Mach–Zehnder interferometer based on microcavities for high-temperature sensing with high sensitivity', Optics letters, 2011, 36, (19), pp. 3753-3755

32 Ymeti, A., Greve, J., Lambeck, P.V., Wink, T., van Hövell, S.W.F.M., Beumer, T.A.M., Wijn, R.R., Heideman, R.G., Subramaniam, V., and Kanger, J.S.: 'Fast, ultrasensitive virus detection using a Young interferometer sensor', Nano letters, 2007, 7, (2), pp. 394-397

33 Bernini, R., Campopiano, S., Zeni, L., and Sarro, P.M.: 'ARROW optical waveguides based sensors', Sensors and Actuators B: Chemical, 2004, 100, (1), pp. 143-146

34 Barrios, C.A.: 'Optical slot-waveguide based biochemical sensors', Sensors, 2009, 9, (6), pp. 4751-4765

35 Zhang, T., Gong, Z., Giorno, R., and Que, L.: 'A nanostructured Fabry-Perot interferometer', Optics express, 2010, 18, (19), pp. 20282-20288

36 Majchrowicz, D., Hirsch, M., Wierzba, P., Bechelany, M., Viter, R., and Jędrzejewska‐Szczerska, M.: 'Application of Thin ZnO ALD Layers in Fiber-Optic Fabry-Pérot Sensing Interferometers', Sensors, 2016, 16, (3), pp. 416

37 Liu, X., Cao, Z., Shen, Q., and Huang, S.: 'Optical sensor based on Fabry-Perot resonance modes', Applied optics, 2003, 42, (36), pp. 7137-7140

38 Qi, Z.-M., Honma, I., and Zhou, H.: 'Nanoporous leaky waveguide based chemical and biological sensors with broadband spectroscopy', Applied physics letters, 2007, 90, (1), pp. 011102

39 Live, L.S., Murray-Methot, M.-P., and Masson, J.-F.: 'Localized and propagating surface plasmons in gold particles of near-micron size', The Journal of Physical Chemistry C, 2008, 113, (1), pp. 40-44

40 Villatoro, J., Monzón-Hernández, D., and Talavera, D.: 'High resolution refractive index sensing with cladded multimode tapered optical fibre', Electronics letters, 2004, 40, (2), pp. 106-107

41 Kieu, K.Q., and Mansuripur, M.: 'Biconical fiber taper sensors', IEEE Photonics Technology Letters, 2006, 18, (21), pp. 2239-2241

42 Laffont, G., and Ferdinand, P.: 'Tilted short-period fibre-Bragg-grating-induced coupling to cladding modes for accurate refractometry', Measurement Science and Technology, 2001, 12, (7), pp. 765

43 Shao, L.-Y., Zhang, A.P., Liu, W.-S., Fu, H.-Y., and He, S.: 'Optical refractive-index sensor based on dual fiber-Bragg gratings interposed with a multimode-fiber taper', IEEE Photonics Technology Letters, 2007, 19, (1), pp. 30-32

44 Wu, Q., Semenova, Y., Wang, P., and Farrell, G.: 'High sensitivity SMS fiber structure based refractometer–analysis and experiment', Optics Express, 2011, 19, (9), pp. 7937-7944

45 Zhang, X., and Peng, W.: 'Bent-fiber intermodal interference based dual-channel fiber optic refractometer', Optics express, 2015, 23, (6), pp. 7602-7610

46 Chen, C.-H., Tsao, T.-C., Tang, J.-L., and Wu, W.-T.: 'A multi-D-shaped optical fiber for refractive index sensing', Sensors, 2010, 10, (5), pp. 4794-4804

47 Wu, S., Yan, G., Zhou, B., Lee, E.-H., and He, S.: 'Open-cavity Fabry–Perot interferometer based on etched side-hole fiber for microfluidic sensing', IEEE Photonics Technology Letters, 2015, 27, (17), pp. 1813

48 Tian, J., Lu, Z., Quan, M., Jiao, Y., and Yao, Y.: 'Fast response Fabry–Perot interferometer microfluidic refractive index fiber sensor based on concave-core photonic crystal fiber', Optics Express, 2016, 24, (18), pp. 20132-20142

49 Caldwell, M.E., and Yeatman, E.M.: 'Surface-plasmon spatial light modulators based on liquid crystal', Applied optics, 1992, 31, (20), pp. 3880-3891

50 Tian, J., Lu, Y., Zhang, Q., and Han, M.: 'Microfluidic refractive index sensor based on an all-silica in-line Fabry–Perot interferometer fabricated with microstructured fibers', Optics express, 2013, 21, (5), pp. 6633-6639

51 Elster, J.L., Jones, M.E., Evans, M.K., Lenahan, S.M., Boyce, C.A., Velander, W.H., and VanTassell, R.: 'Optical fiber extrinsic Fabry-Perot interferometric (EFPI)-based biosensors', in Editor (Ed.)^(Eds.): 'Book Optical fiber extrinsic Fabry-Perot interferometric (EFPI)-based biosensors' (International Society for Optics and Photonics, 2000, edn.), pp. 105-112

52 Xiao, G.Z., Adnet, A., Zhang, Z., Sun, F.G., and Grover, C.P.: 'Monitoring changes in the refractive index of gases by means of a fiber optic Fabry-Perot interferometer sensor', Sensors and Actuators A: Physical, 2005, 118, (2), pp. 177-182

53 Martini, J., Kiesel, P., Roe, J., and Bruce, R.H.: 'Glucose concentration monitoring using a small Fabry-Pérot etalon', Journal of biomedical optics, 2009, 14, (3), pp. 034029-034029-034028

54 bin Mat Yunus, W.M., and bin Abdul Rahman, A.: 'Refractive index of solutions at high concentrations', Applied optics, 1988, 27, (16), pp. 3341-3343

55 Solanki, J., Choudhary, O.P., Sen, P., and Andrews, J.T.: 'Polarization sensitive optical low-coherence reflectometry for blood glucose monitoring in human subjects', Review of Scientific Instruments, 2013, 84, (7), pp. 073114

56 Fang, Y.-L., Wang, C.-T., and Chiang, C.-C.: 'A Small U-Shaped Bending-Induced Interference Optical Fiber Sensor for the Measurement of Glucose Solutions', Sensors, 2016, 16, (9), pp. 1460

57 Larin, K.V., Akkin, T., Esenaliev, R.O., Motamedi, M., and Milner, T.E.: 'Phase-sensitive optical low-coherence reflectometry for the detection of analyte concentrations', Applied optics, 2004, 43, (17), pp. 3408-3414

58 Larin, K.V., Akkin, T., Milner, T.E., Dave, D.P., Motamedi, M., and Esenaliev, R.O.: 'Measurement of refractive index variation of physiological analytes using differential-phase OCT', in Editor (Ed.)^(Eds.): 'Book Measurement of refractive index variation of physiological analytes using differential-phase OCT' (International Society for Optics and Photonics, 2004, edn.), pp. 31-34

59 Chong, J.H., Shum, P., Haryono, H., Yohana, A., Rao, M., Lu, C., and Zhu, Y.: 'Measurements of refractive index sensitivity using long-period grating refractometer', Optics Communications, 2004, 229, (1), pp. 65-69

60 Paliwal, A., Sharma, A., Tomar, M., and Gupta, V.: 'Long range surface plasmon resonance (LRSPR) based highly sensitive refractive index sensor using Kretschmann prism coupling arrangement', in Editor (Ed.)^(Eds.): 'Book Long range surface plasmon resonance (LRSPR) based highly sensitive refractive index sensor using Kretschmann prism coupling arrangement' (AIP Publishing, 2016, edn.), pp. 020132

61 Marzuki, A., and Sari, N.W.: 'Design of reflective optical fiber sensor for determining refractive index and sugar concentration of aqueous solutions', in Editor (Ed.)^(Eds.): 'Book Design of reflective optical fiber sensor for determining refractive index and sugar concentration of aqueous solutions' (IOP Publishing, 2016, edn.), pp. 012032

62 Hernández-Arriaga, M.V., Bello-Jiménez, M.A., Rodríguez-Cobos, A., and Andrés, M.V.: 'Experimental Investigation of Fused Biconical Fiber Couplers for Measuring Refractive Index Changes in Aqueous Solutions', IEEE Sensors Journal, 2016, 16, (1), pp. 132-136

63 Liu, C., Cai, Q., Sun, Z., Xu, B., Zhao, J., Zhang, L., and Chen, X.: 'Fibre optic chemical sensor based on graphene oxide-coated long period grating', in Editor (Ed.)^(Eds.): 'Book Fibre optic chemical sensor based on graphene oxide-coated long period grating' (International Society for Optics and Photonics, 2016, edn.), pp. 99160V-99160V-99164

64 Shih, M.C., Yang, H.-H., and Shih, C.H.: 'Measurement of the index of refraction of an liquid by a cladding depleted fiber Bragg grating', Optical and Quantum Electronics, 2016, 48, (2), pp. 1-6

65 Bhatia, V., Murphy, K.A., Claus, R.O., Jones, M.E., Grace, J.L., Tran, T.A., and Greene, J.A.: 'Optical fibre based absolute extrinsic Fabry-Perot interferometric sensing system', Measurement Science and Technology, 1996, 7, (1), pp. 58

66 Murphy, K.A., Gunther, M.F., Vengsarkar, A.M., and Claus, R.O.: 'Quadrature phase-shifted, extrinsic Fabry–Perot optical fiber sensors', Optics letters, 1991, 16, (4), pp. 273-275

67 Jaeger, H., Mercer, P., and Sherwood, R.: 'The effect of exposure to air on silver and gold films deposited in ultra-high vacuum', Surface Science, 1969, 13, (2), pp. 349-360

68 Pettersson, L., and Snyder, P.: 'Preparation and characterization of oxidized silver thin films', Thin Solid Films, 1995, 270, (1), pp. 69-72

69 Erb, R.A.: 'Wettability of metals under continuous condensing conditions', The Journal of Physical Chemistry, 1965, 69, (4), pp. 1306-1309

70 Sankar, S., Nair, B.N., Suzuki, T., Anilkumar, G.M., Padmanabhan, M., Hareesh, U.N.S., and Warrier, K.G.: 'Hydrophobic and Metallophobic Surfaces: Highly Stable Non-wetting Inorganic Surfaces Based on Lanthanum Phosphate Nanorods', Scientific reports, 2016, 6

71 http://slideplayer.com/slide/11344425/ [1 CHAPTER 1 Wave Nature of Light. 2 1.1 LIGHT WAVES IN HOMOGENEOUS MEDIUM.Published byClifford Norris] Last downloaded 20th July 2017

72 University, S.D.S.: 'EE 766: Thin Film Materials and Devices', in Editor (Ed.)^(Eds.): 'Book EE 766: Thin Film Materials and Devices' (2016 Spring, edn.), pp.

73 Hernandez, G.: 'Fabry-perot interferometers' (Cambridge University Press, 1988. 1988)

74 http://www.polifab.polimi.it/equipments/magnetron-sputtering-system-leybold-lh-z400/[Magnetron Sputtering System LEYBOLD LH Z400] Last downloaded 20th July'17

75 Ekem, N., Korkmaz, S., Pat, S., Balbag, M., Cetin, E., and Ozmumcu, M.: 'Some physical properties of ZnO thin films prepared by RF sputtering technique', International Journal of Hydrogen Energy, 2009, 34, (12), pp. 5218-5222

76 Rajurkar, K., Zhu, D., McGeough, J., Kozak, J., and De Silva, A.: 'New developments in electro-chemical machining', CIRP Annals-Manufacturing Technology, 1999, 48, (2), pp. 567-579

77 Rajurkar, K., Sundaram, M., and Malshe, A.: 'Review of electrochemical and electrodischarge machining', Procedia CIRP, 2013, 6, pp. 13-26

78 Wuthrich, R., and Ziki, J.D.A.: 'Micromachining using electrochemical discharge phenomenon: fundamentals and application of spark assisted chemical engraving' (William Andrew, 2014. 2014)

79 Wüthrich, R., and Fascio, V.: 'Machining of non-conducting materials using electrochemical discharge phenomenon—an overview', International Journal of Machine Tools and Manufacture, 2005, 45, (9), pp. 1095-1108

80 'EE 560 Sensors and measurement', in Editor (Ed.)^(Eds.): 'Book EE 560 Sensors and measurement' (South Dakota State University, 2016 Spring, edn.), pp.

81 Proksche, H., Nagorsen, G., and Ross, D.: 'The Influence of NH 4 F on the Etch Rates of Undoped SiO2 in Buffered Oxide Etch', Journal of the Electrochemical Society, 1992, 139, (2), pp. 521-524

82 Spierings, G.: 'Wet chemical etching of silicate glasses in hydrofluoric acid based solutions', Journal of Materials Science, 1993, 28, (23), pp. 6261-6273

83 Knotter, D.M.: 'Etching mechanism of vitreous silicon dioxide in HF-based solutions', Journal of the American Chemical Society, 2000, 122, (18), pp. 4345-4351

84 Williams, K.R., and Muller, R.S.: 'Etch rates for micromachining processing', Journal of Microelectromechanical systems, 1996, 5, (4), pp. 256-269

85 Webster, J.: 'Medical instrumentation: application and design' (John Wiley & Sons, 2009. 2009)

86 Garces, F.O.: 'UV Visible Absorption Spectroscopy', Available: http://faculty.sdmiramar.edu/fgarces/LabMatters/Instruments/UV_Vis/Cary50.htm

87 Zhao, W.: 'Contact angle measurement', 2015

88 Kwok, D.Y., and Neumann, A.W.: 'Contact angle measurement and contact angle interpretation', Advances in colloid and interface science, 1999, 81, (3), pp. 167-249

89 Decker, E., Frank, B., Suo, Y., and Garoff, S.: 'Physics of contact angle measurement', Colloids and Surfaces A: Physicochemical and Engineering Aspects, 1999, 156, (1), pp. 177-189

90 Ennaceri, H., Benyoussef, A., Ennaoui, A., and Khaldoun, A.: 'Optical Properties of Front and Second Surface Silver-Based and Molybdenum-Based Mirrors', International Journal of Engineering and Technology, 2016, 8, (6)

91 Martın-Palma, R.J., and Martınez-Duart, J.M.: 'Accurate determination of the optical constants of sputter-deposited Ag and SnO2 for low emissivity coatings', Journal of Vacuum Science & Technology A, 1998, 16, (2), pp. 409-412

92 Ni, C., Shah, P., and Sarangan, A.M.: 'Effects of different wetting layers on the growth of smooth ultra-thin silver thin films', in Editor (Ed.)^(Eds.): 'Book Effects of different wetting layers on the growth of smooth ultra-thin silver thin films' (International Society for Optics and Photonics, edn.), pp. 91700L-91700L

93 Machida, M., Norimoto, K., Watanabe, T., Hashimoto, K., and Fujishima, A.: 'The effect of SiO2 addition in super-hydrophilic property of TiO2 photocatalyst', Journal of Materials science, 1999, 34, (11), pp. 2569-2574

94 Yu, J., Zhao, X., Yu, J.C., Zhong, G., Han, J., and Zhao, Q.: 'The grain size and surface hydroxyl content of super-hydrophilic TiO2/SiO2 composite nanometer thin films', Journal of materials science letters, 2001, 20, (18), pp. 1745-1748

95 Masteika, V., Kowal, J., Braithwaite, N.S.J., and Rogers, T.: 'A review of hydrophilic silicon wafer bonding', ECS Journal of Solid State Science and Technology, 2014, 3, (4), pp. Q42-Q54

96 Suni, T., Henttinen, K., Suni, I., and Mäkinen, J.: ‘Effects of plasma activation on hydrophilic bonding of Si and SiO2’, Journal of the Electrochemical Society, 2002, 149, (6), pp. G348-G351

97 Wu, D.K., Kuhlmey, B.T., and Eggleton, B.J.: ‘Ultrasensitive photonic crystal fiber refractive index sensor’, Optics letters, 2009, 34, (3), pp. 322-324

98 Zhang, W., Wang, R., Rong, Q., Qiao, X., Guo, T., Shao, Z., Li, J., and Ma, W.: ‘An Optical Fiber Fabry–Perot Interferometric Sensor Based on Functionalized Diaphragm for Ultrasound Detection and Imaging’, IEEE Photonics Journal, 2017, 9, (3), pp. 1-8

99 Ou, Y., Zhou, C., Zheng, A., Cheng, C., Fan, D., Yin, J., Tian, H., Li, M., and Lu, Y.: ‘Method of hybrid multiplexing for fiber-optic Fabry–Perot sensors utilizing frequency-shifted interferometry’, Applied optics, 2014, 53, (35), pp. 8358-8365

100 Sobral, H., and Peña-Gomar, M.: ‘Determination of the refractive index of glucose-ethanol-water mixtures using spectroscopic refractometry near the critical angle’, Applied optics, 2015, 54, (28), pp. 8453-8458

101 Crespi, A., Gu, Y., Ngamsom, B., Hoekstra, H.J., Dongre, C., Pollnau, M., Ramponi, R., van den Vlekkert, H.H., Watts, P., and Cerullo, G.: ‘Three-dimensional Mach-Zehnder interferometer in a microfluidic chip for spatially-resolved label-free detection’, Lab on a Chip, 2010, 10, (9), pp. 1167-1173

102 Friebel, M., and Meinke, M.: ‘Model function to calculate the refractive index of native hemoglobin in the wavelength range of 250-1100 nm dependent on concentration’, Applied optics, 2006, 45, (12), pp. 2838-2842

103 Sydoruk, O., Zhernovaya, O., Tuchin, V., and Douplik, A.: ‘Refractive index of solutions of human hemoglobin from the near-infrared to the ultraviolet range: Kramers-Kronig analysis’, Journal of biomedical optics, 2012, 17, (11), pp. 115002-115002